

P38-ALPHA INHIBITION BY ROOPEROL: DOCKING AND  
KINASE ASSAY STUDIES

by

Blanca Virginia Estevez Posadas B. S.

A thesis submitted to the Graduate Council of  
Texas State University in partial fulfillment  
of the requirements for the degree of  
Master of Science,  
with a Major in Chemistry  
August 2021

Committee Members:

Sean M. Kerwin

Wendi M. David

Karen A. Lewis

**COPYRIGHT**

by

Blanca Virginia Estevez Posadas

2021

## **FAIR USE AND AUTHOR'S PERMISSION STATEMENT**

### **Fair Use**

This work is protected by the Copyright Laws of the United States (Public Law 94-553, section 107). Consistent with fair use as defined in the Copyright Laws, brief quotations from this material are allowed with proper acknowledgement. Use of this material for financial gain without the author's express written permission is not allowed.

### **Duplication Permission**

As the copyright holder of this work I, Blanca Virginia Estevez Posadas, authorize duplication of this work, in whole or in part, for educational or scholarly purposes only

## **ACKNOWLEDGEMENTS**

I would like to give my most sincere acknowledgement to my research advisor Dr. Sean M. Kerwin for all his help, and patience with me in the accomplishment of this work. Also, I would like to thank him for all the knowledge he helped me acquire during my time as a master student. I would also like to thank to my committee members Dr. Karen Lewis and Dr. Wendi David for all their support and advice that helped me to improve as a student and as a researcher. Finally, I would like to thank to the members of the Kerwin lab, and to Chelsea Davis, for all their support when I needed it the most inside and outside the lab. Likewise, to all of those that have made possible this work, my most sincere gratitude.

## TABLE OF CONTENTS

	<b>Page</b>
ACKNOWLEDGEMENTS.....	iv
LIST OF TABLES.....	vii
LIST OF FIGURES.....	viii
LIST OF ABBREVIATIONS.....	x
ABSTRACT.....	xii
CHAPTERS	
I. INTRODUCTION.....	1
1. Kinases and Their Importance.....	1
2. Protein Kinases as Drug Targets.....	2
3. Promiscuous Inhibitors.....	4
4. MAP Kinases.....	6
5. p38 $\alpha$ MAP Kinase.....	8
6. p38 $\alpha$ MAPK Docking Recruitment Site (DRS).....	11
7. Rooperol.....	12
8. Metabolism and Activity of Rooperol.....	13
9. Rooperol and Analogues.....	15
10. Protein Kinase Docking Approaches in Virtual Screening and Inhibitor Characterization.....	17
11. Binding Assays for Protein Kinase Ligands.....	19
12. Research Aims .....	21
II. EXPERIMENTAL.....	22
1. Materials & Instruments .....	22
2. Computational 3D Modeling.....	23
2.1. Methodology.....	23
3. Horseradish Peroxidase Assay.....	24
3.1. Preparation of Stock Solutions .....	24
3.2. Standard Curves.....	25

4. Standardization of The ADP-Glow Reaction.....	28
4.1. Preparation of Stock Solutions.....	31
4.2. Standard Curves.....	35
III. RESULTS & DISCUSSION.....	46
1. Computational 3D Modeling.....	46
2. Horseradish Peroxidase Assay.....	49
3. Standardization of The ADP-Glow Reaction.....	58
IV. CONCLUSIONS.....	70
LITERATURE CITED.....	72

## LIST OF TABLES

<b>Table</b>	<b>Page</b>
1: HRP enzyme units on the serial dilutions.....	26
2: Modes to dispense and to aspirate of the pipetting robot.....	28
3: Way in which the plate was filled in part fourth of the HRP assay.....	28
4: meaning of the Z' values.....	29
5: ATP-ADP conversion curve (first attempt).....	36
6: Concentrations of HK dilutions.....	37
7: DMSO concentrations.....	39
8: ATP dilutions for correction of ATP-ADP curve.....	40
9: Dilutions of ADP in ATP to obtain the corrected ATP-ADP percent conversion curve.....	40
10: Serial dilutions of p38 $\alpha$ .....	42
11: Concentrations of MBP.....	43
12: Staurosporine dilutions.....	44
13: Rooperol affinity with the alternative groove against affinity with the DRS .....	48

## LIST OF FIGURES

Figure	Page
1: Human kinome for protein kinases.....	2
2: Human kinome and targeted protein kinases.....	4
3: Human kinome for protein kinases and promiscuous inhibitors.....	6
4: MAPK activation.....	8
5: Process of activation of p38 $\alpha$ and the biological response after its activation.....	10
6: (A) DRS site (pink) in p38 $\alpha$ and the MEF2A KIM peptide (green).....	12
7: The African potato and the chemical structure of hypoxoside and rooperol.....	13
8: Rooperol and phase II metabolites.....	14
9: Rooperol analogues.....	16
10: Alternative groove's box in p38 $\alpha$ . (1LEW crystal structure).....	46
11: Localization of the alternative groove and the DRS site in the 1LEW p38 $\alpha$ crystal structure.....	47
12: Docking between rooperol and the alternative groove in the crystal structure 1LEW of p38 $\alpha$ .....	48
13: Luminescence displayed by HRP at different concentrations for a period of one hour at room temperature.....	50
14: Luminescence displayed by HRP at different concentrations for a period of one hour at room temperature.....	51
15: Luminescence displayed by HRP (0.625 mU) for a period of one hour at room temperature.....	52
16: Luminescence displayed by HRP (0.625 mU) for a period of one hour at room temperature.....	53

17: Luminescence displayed by HRP (0.625mU) against buffer for a period of one hour at room temperature.....	54
18: Luminescence displayed by HRP (0.625 mU) against buffer for a period of one hour at room temperature.....	54
19: Comparison of the five different modes of dispensing HRP solution.....	56
20: Comparison of the relative error of the five different modes of dispensing HRP solution when using 40 $\mu$ L of mixing volume.....	57
21: Example of the ATP-ADP conversion curve obtained during the first attempt to reproduce Zegzouti H results.....	59
22 Example of the HK curve obtained during the first attempt to reproduce Zegzouti H results.....	60
23: ATP-ADP conversion curve obtained during the second attempt to reproduce Zegzouti H results.....	61
24: HK conversion curve obtained during the second attempt to reproduce Zegzouti H results.....	62
25: ATP-ADP conversion curve obtained during the second step (measuring DMSO effect).....	63
26: DMSO effect in the ADP-Glow reaction.....	63
27: Second correction of the ATP-ADP percent conversion curve.....	64
28: p38 $\alpha$ conversion curve at a constant concentration of MBP.....	66
29: p38 $\alpha$ conversion curve with different concentration of MBP.....	67
30: p38 $\alpha$ conversion curve with different concentration of staurosporine.....	69

## LIST OF ABBREVIATIONS

<b>Abbreviation</b>	<b>Description</b>
ATP	Adenosine triphosphate
ADP	Adenosine diphosphate
DRS	Docking recruitment site
3D	3 dimensions
HTS	High throughput screening
Z'	Z' factor
S/N	Signal to noise ratio
S/B	Signal to baseline ratio
Ser	Serine
Thr	Threonine
MAPK	Mitogen activated protein kinase
ERKs	Extracellular-signal-regulated kinases
JNKs	Jun amino-terminal kinases
SAPKs	Stress-activated protein kinases
KIM-motif	Kinase interaction motif
Tyr	Tyrosine
UV	Ultraviolet light.
RNA	Ribonucleic acid
T1/2	Half life

VS	Virtual screening
LVS	Ligand-based virtual screening
SVS	Structure-based virtual screening
ELISA	Enzyme-linked immunosorbent assay
4IPBA	4- Iodophenylboronic acid
DMSO	Dimethyl sulfoxide
HRP	Horseradish peroxidase
BSA	Bovine serum albumin
DTT	Dithiothreitol
MBP	Myelin basic protein
HK	Hexokinase
PDB	Protein data bank

## ABSTRACT

p38 $\alpha$  is a protein kinase with a high importance in cell metabolism due to its role in inflammation, apoptosis, differentiation, and cell cycle regulation. It is activated by a cascade of reactions that starts with cytokines, growth factors, and a variety of cellular stresses. p38 $\alpha$  also has a main role in cancer cells, therefore, its inhibition is of great importance for cancer treatments. There have been many attempts to develop inhibitors for p38 $\alpha$ , most of them target the conserved ATP active site. Since the inhibitors that target this site compete with the ATP, the efficacy of inhibiting p38 $\alpha$  is reduced. Therefore, it is crucial to find molecules that inhibit p38 $\alpha$  by targeting allosteric active sites. Rooperol is a natural product obtained from the African potato that has shown inhibitory activity against p38 $\alpha$  by targeting the allosteric DRS active site. Nevertheless, this molecule has a short half-life in the human metabolism. Therefore, it is essential to obtain p38 $\alpha$  inhibitors from rooperol analogues that last longer in the human metabolism. To measure the inhibition performed by such analogues, it is necessary to standardize an assay to measure the percent inhibition. Nowadays, there are some assays already developed to measure protein kinase enzyme inhibition. One of the most used techniques requires radioactive labeling of ATP with  $^{33}\text{P}$  or  $^{32}\text{P}$ . This technique provides direct measurement of the incorporation of phosphorous by protein kinase substrates and few sources of interference, but the risk of using radioactive materials leads hazards that must be managed during the reaction and special waste disposal. Therefore, non-radioactive assays are also well used such as fluorescent and luminescent endpoint assays.

Nevertheless, these techniques also have some disadvantages such as high interference, and specific requirements of antibody reagents. Hence, there is great necessity to standardize such assays with the specific requirements for each enzyme. In this work, the region(s) of the p38 $\alpha$  DRS that are most likely bound by rooperol are investigated. Also, the universal ATP-Glow kinase assay for use on a pipetting robot to determine protein kinase inhibition was miniaturized and adapted. The results obtained in this work are described in two parts. Firstly, the computational 3D modeling. Secondly, the miniaturization and standardization of the ADP-Glow reaction. The 3D modeling was performed using computational software such as AutoDockTools, Vina, and Chimera. This analysis was performed to measure the affinity of rooperol to an active site in p38 $\alpha$  close to the DRS site (the alternative groove) in 9 different crystal structures of the p38 $\alpha$  enzyme. The predicted affinity results obtained ranged from -5.2 to -6.1 kcal/mol. These results show a moderate affinity between the alternative groove and rooperol. Nevertheless, they are significantly inferior to the results obtained from the DRS site that ranged from -6.5 to -7.3 kcal/mol (results obtained from another member of the research group). Thus, the alternative groove did not show a greater affinity as the DRS site and should not be further explored. In the second part of the results, the changes made to the ADP-Glow reaction to standardize, minimize, and adapt it for HTS were measured by Z-factor, S/N (signal to noise), S/B (signal to base line), and R<sup>2</sup>. The results obtained were 0.9, 430, 141, and 0.981, respectively. These results showed that the standardized assay is excellent.

## I. INTRODUCTION

### 1. Kinases and Their Importance

Protein kinases are one of the most extensive signaling groups in the eukaryotic cells. They form a very large family of enzymes for more than 500 members<sup>1</sup>. They are critical in metabolism, cell signaling, protein regulation, cellular transport, and secretory means since they are involved in almost all cellular processes. Their physiological role in cells is to transfer a phosphate group from a phosphate donor on to a variety of substrate proteins<sup>2</sup>. Most kinases are Ser/Thr protein kinases; they phosphorylate Ser/Thr residues of their substrates. Such kinases are capable to phosphorylate other enzymes, including other kinases, transcription factors, receptors, and other regulatory proteins<sup>3</sup>. In figure 1, the human kinome map for kinases shows the six groups of protein kinases: the AGC group, the CaMK group (for calcium-calmodulinindependent), the CMGC group (for CDK, MAP kinase, glycogen synthase kinase, and CDK-like), the STE group (homologues of STE11 and STE20), the CK1 group (for casein kinase-1), and TKL (tyrosine kinase like)<sup>1 3</sup>. This classification is based on the acceptor amino acid specificity of the protein kinases, in other words, they are classified based on the amino acid sequence of their catalytic domains<sup>2 4</sup>.

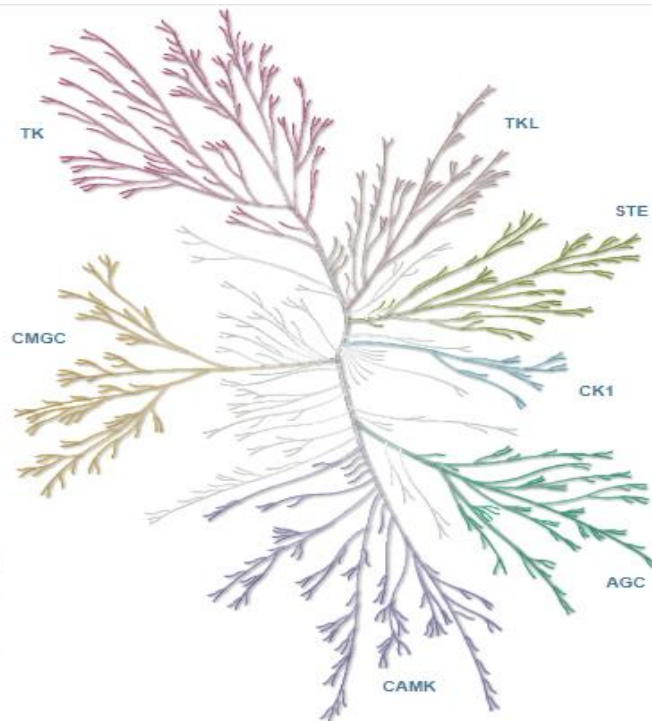


**Figure 1: Human kinome for protein kinases.** Each one of the branches represents a specific protein kinase<sup>2</sup>, and they are grouped in 7 classes: CAMK, AGC, CK1, STE, TKL, TK, and CMGC.

## 2. Protein Kinases as Drug Targets

Given the role and the importance of the protein kinases to maintain the equilibrium in the cells, many protein kinases are targets for drug discovery and drug development. Transportation of a phosphorus group from one molecule to another is one of the most important means of signaling from outside of the cellular membrane to the nucleus<sup>5</sup>. Kinases are in charge of such delicate tasks and when alterations in their signaling pathway arise they trigger many different diseases such as cancer, diabetes, neurodegeneration, and inflammation<sup>5 6 7</sup>. Therefore, to find a cure for such diseases, the development of drugs that inhibit or regulate protein kinases have increased in the last decades.

Members of the protein kinase families are important targets to develop drugs due to the specific and temporal manner of activation of these enzymes. Most of the protein kinases share part of their amino acid sequence among families, nevertheless, their activation occurred in a grade of specificity. For instance, p38 $\alpha$  MAPK has four isoforms ( $\alpha$ ,  $\beta$ ,  $\gamma$ , and  $\delta$ ), they share the 60% of their amino acid sequence but they have important differences in tissue expression as well in ways of activation and inactivation<sup>8</sup>. Most importantly, these enzymes have different responses to chemical inhibitors. p38 $\alpha$  and p38 $\beta$  are inhibited by pyridinyl imidazole compounds<sup>9</sup>, while p38 $\gamma$  and p38 $\delta$  are insensitive to such inhibitors<sup>10</sup>. Thus, it is possible to take advantage of the specificity of MAPKs to develop drugs that inhibit or regulate a specific enzyme.

Despite the importance and advantages that MAPKs represent as drug targets, there is still a great gap of knowledge when talking about inhibitors. Most of the key targets of approved drugs are members of the TK family (figure 2). There are few drugs that target the CMGC family (to which p38 $\alpha$  belongs) and in the best of our knowledge there is not an approved drug that targets p38 $\alpha$ .

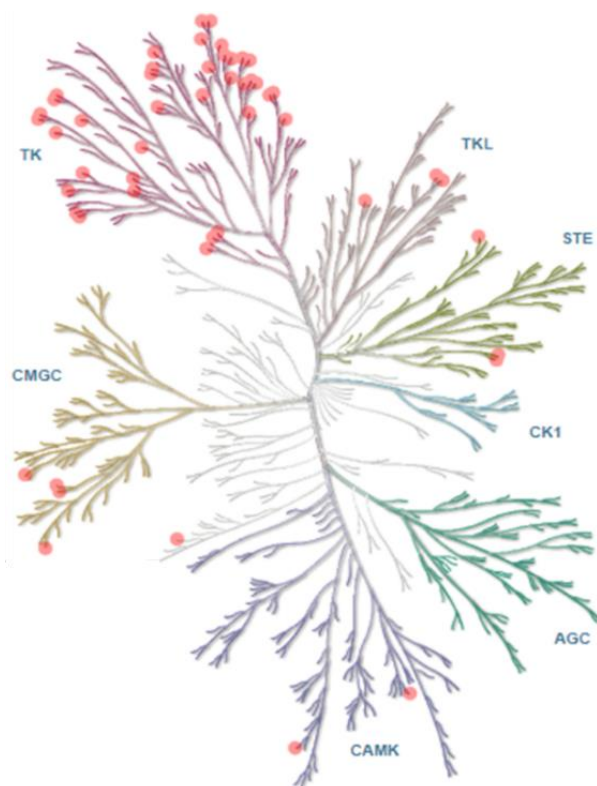


**Figure 2: Human kinome and targeted protein kinases.** The red dots highlight the kinases that already have approved inhibitors in the market <sup>11</sup>. The kinases that are part of the TK class are the kinases with more inhibitors in the market.

### 3. Promiscuous Inhibitors

Kinase inhibition is an important tool to adjust several pathological disequilibria in cells. Kinases are important for cell life because they control differentiation, proliferation, apoptosis, metabolism, and immunological responses in the cell. Therefore, the diseases related to kinase disequilibria can be treated with a kinase inhibitor. There are 7 groups of inhibitors. Type I inhibitors bind to the active conformation of kinases. Type II/2 bind to the DFG-D in,  $\alpha$ C-helix out conformation of kinases but the compound can extend to the back of the enzyme and have interactions with pockets involved in the type II inhibition. Type II inhibitors bind to the inactive conformations of kinases. Type III and IV involve allosteric inhibitors. Type III binds within a cleft adjacent to the ATP-

site, and Type IV binds elsewhere. Type V inhibitors are bivalent molecules that bind to two regions of the protein kinase domain. Finally, Type VI are covalent kinase inhibitors<sup>12</sup>. However, most of the kinase inhibitors developed until now are type I inhibitors. Thus, they target the ATP binding pocket which is highly conserved across kinases making difficult to inhibit one specific kinase<sup>13</sup>.

This is an important issue due to the different roles of kinases. On the other hand, developing an inhibitor that targets a specific kinase is very challenging. In the research conducted by Gonzalez-Medina (2020)<sup>14</sup>, 637 inhibitors, specific for p38 $\alpha$  that target the ATP binding site, were tested for promiscuity. 19% of those inhibitors were promiscuous at a determined limit of activity for p38 $\alpha$  (Figure 3). In that study, it was found that most of the inhibitors for p38 $\alpha$  have great degree of selectivity despite that their targeted site is the ATP.

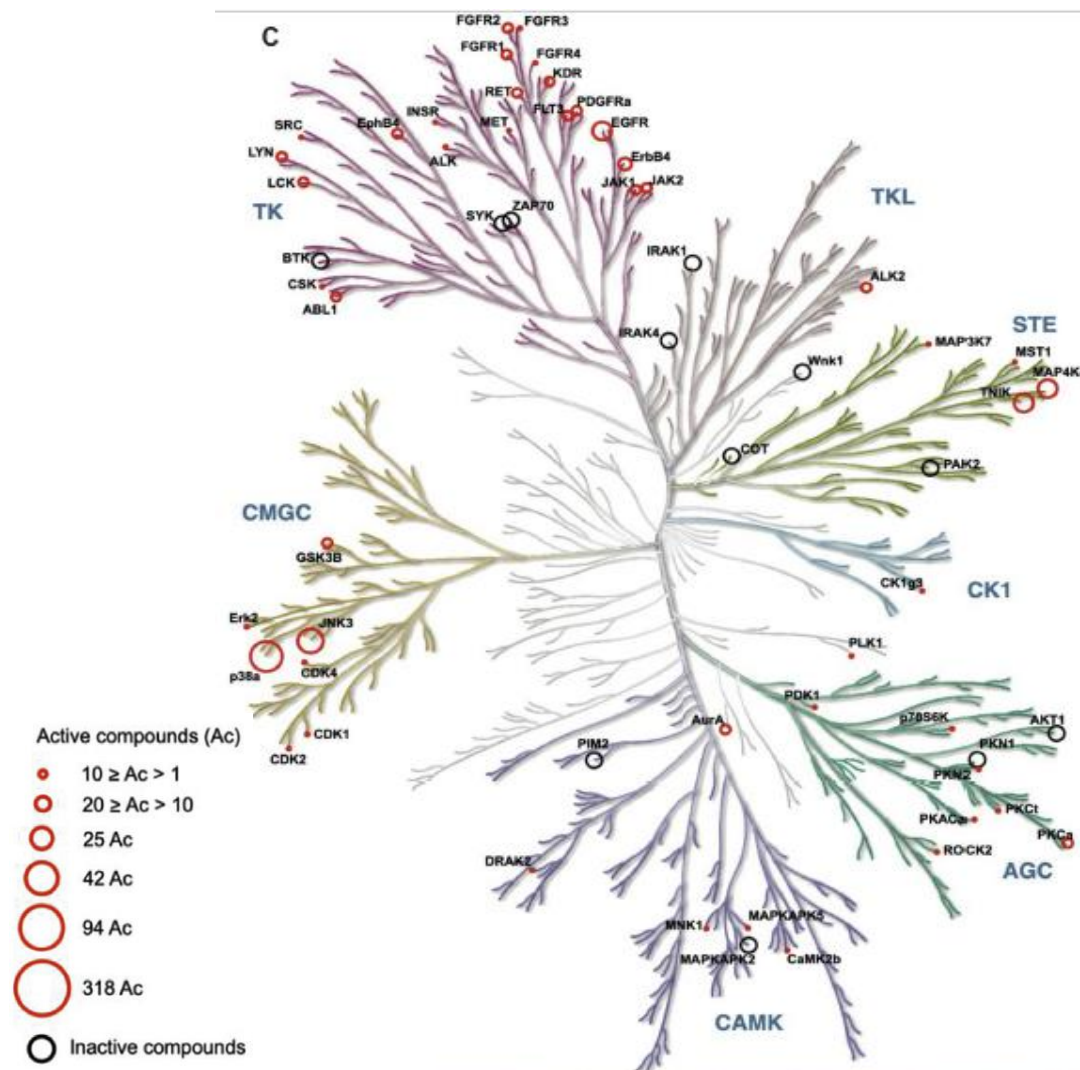


**Figure 3: Human kinome for protein kinases and promiscuous inhibitors.** Red circles shows the kinases inhibited by promiscuous inhibitors of p38 $\alpha$ . Black circles shows kinases that are not inhibited by p38 $\alpha$  inhibitors<sup>14</sup>.

#### 4. MAP Kinases

Mitogen-Activated Protein Kinases (MAPK) are kinases that are activated in a cascade of reactions induced by other kinases. The modules of the MAPK contain a sequence of three kinases (Figure 4), the first kinase (MAPKKK: MAP kinase kinase kinase) activates the next kinase (MAPKK: MAP kinase kinase) which activates the next kinase (MAPK: MAP kinase)<sup>5 15</sup>. MAP Kinases, the last scaffold of the cascade, are

activated by dual phosphorylation in their threonine and tyrosine residues which are located in the phosphorylate loop<sup>16</sup>. Then they are dephosphorylated by dual specificity phosphatases (DUSPs)<sup>17</sup>. The MAP kinases can be classified into three main families: ERKs (extracellular-signal-regulated kinases), JNKs (jun amino-terminal kinases), and p38/SAPKs (stress-activated protein kinases)<sup>15</sup>. These important families accomplish the function of translate extracellular signs such as growth factors and stress into specific intracellular responses like cellular differentiation, inflammation, and apoptosis<sup>5 18</sup>.

The structure of MAPKs is well known in detail. MAPKs are constructed by two lobes. They have five-stranded  $\beta$ -sheet in the N-terminal lobe and six  $\alpha$ -helices in the C-terminal lobe<sup>19 20</sup>. The majority of MAPKs contains a docking site in the C-terminal lobe known as D- or KIM-motif (kinase interaction motif) which consist of 13-16 amino acids<sup>21</sup>. In most of the cases the KIM motif is followed by the dual-specificity kinase domain, together they control the activity of MAKs; the active and inactive states<sup>22</sup>.

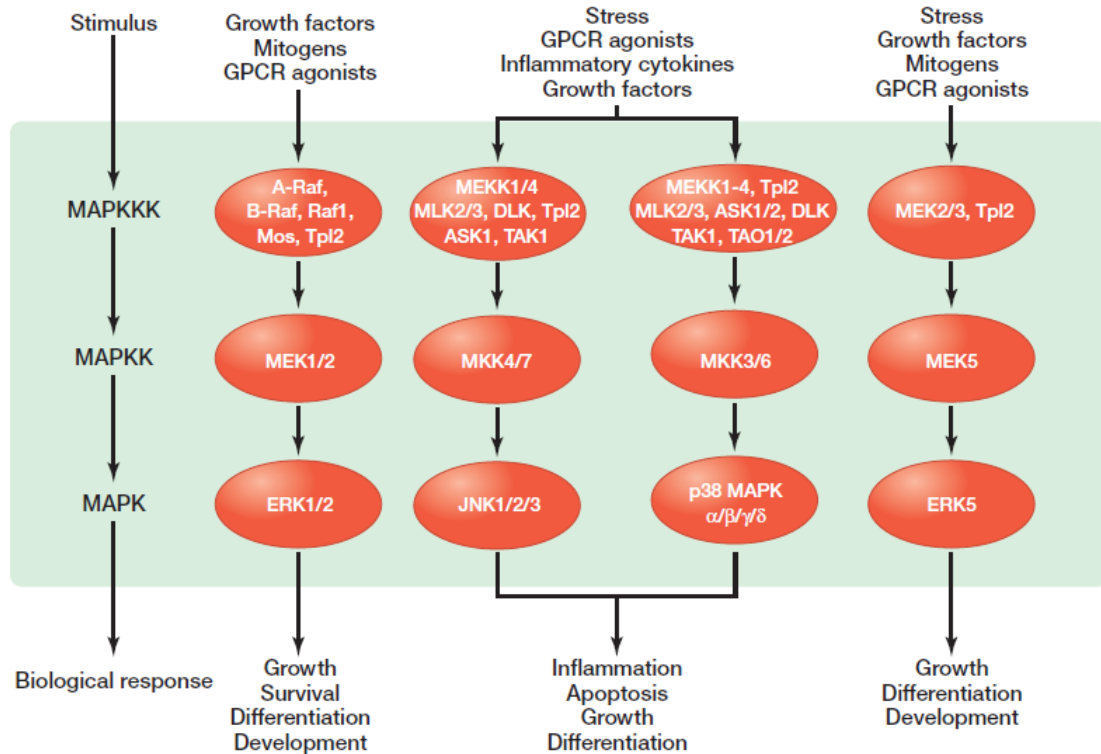


**Figure 4: MAPK activation** <sup>15</sup>.

## 5. p38 $\alpha$ MAP Kinase

MAP kinases p38 $\alpha$  have an important role in inflammation, apoptosis, cell differentiation, and cell cycle regulation. The cascade of p38 $\alpha$  is activated by cytokines, growth factors, and a variety of cellular stresses, including UV and, ionizing radiation, hyperosmolarity, and heat shock <sup>23</sup> (Figure 5). p38 $\alpha$  MAPK is phosphorylated on Tyr180 and Thr182 by the upstream MAP kinase kinase 3 (MKK3) and MAP kinase kinase 6 (MKK6) leading to its activation <sup>24</sup>. This phosphorylation leads to a conformational change that enables catalytic transfer of a phosphate from ATP to the substrate protein <sup>8</sup>. The endurance of the phosphorylated state of p38 $\alpha$  has a relation between apoptosis and cell life, for instance, prolonged activation state of p38 $\alpha$  has been linked with induction of cell apoptosis <sup>25</sup>. The duration of the activated state is regulated by phosphatases, such

as protein phosphatase 1, protein phosphatase 2A or MAPK phosphatases<sup>17</sup>. ATF-2, Elk-1, Max, and the kinases MAPKAP-2/3 and MNK1/2 are the species activated by the downstream cascade of p38 $\alpha$ <sup>23</sup>. The downstream effects of p38 $\alpha$  are different depending on the type of cell in which the process is taking place. These effects could be inflammatory responses, cell differentiation, cell-cycle arrest, apoptosis, senescence, cytokine production and regulation of RNA splicing<sup>8</sup>.

Lately, p38 $\alpha$  has been the object of several studies due to its relation to diseases with inflammatory components such as rheumatoid arthritis, Crohn's disease, psoriasis, asthma, and cancer. Rheumatoid arthritis is a common autoimmune and inflammatory disease. During this disease various joints of the body are affected at the same time such as hands, wrists, and knees. In a joint affected, the lining presents inflammation, and it can cause harm to the joint tissue<sup>26</sup>. The four isoforms of p38 have been found in the synovial membrane of a joint affected by rheumatoid arthritis with p38 $\alpha$  and  $\gamma$ , the isoforms with major presence in the affected tissues being linked to chronic inflammation<sup>27</sup>.

Another disease that has inflammation characteristics related to the effects of p38 $\alpha$  is Crohn's disease. This disease is characterized by the transmural granulomatous inflammation of all the digestive tract and principally the ileum and colon. This is a recidivist of inflammatory bowel disease (IBD)<sup>28</sup>. In this disease cytokines play an important role activating p38 MAPKs. This activity can be observed by the increase presence of p38 MAPK in the inflamed colonic mucosa of patients with Crohn's disease (CD)<sup>8</sup>.

p38 MAPKs are important in cancer development. Cancer is a disease characterized by cells avoiding apoptosis, cell unlimited reproduction, tissue invasion and metastases, angiogenesis, evasion of replicative senescence and generation of drug resistance<sup>29</sup>. The major proof of the role of p38 MAPKs in the development of cancer comes from studies of cell lines and mouse knockout models where inactivation of these enzymes enhances tumor suppression<sup>30</sup>. When p38 $\alpha$  and  $\beta$  are inhibited on different cell tissues, the cellular growth is diminished and the induction of apoptosis is increased<sup>30</sup> as well as senescence<sup>31</sup>. Therefore, the importance of p38 $\alpha$  as a drug target relies on its role in autoimmune and inflammation diseases as well in cancer.

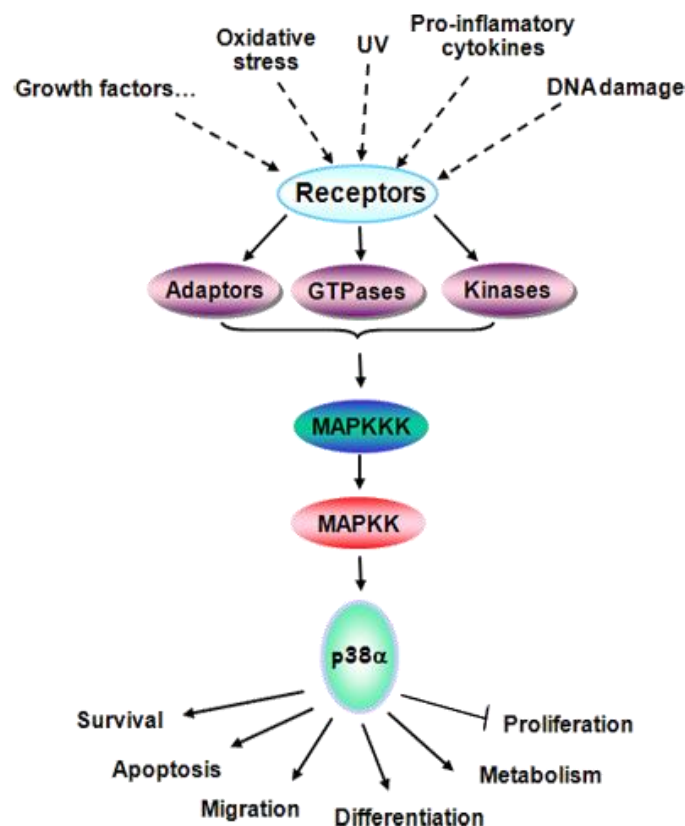


**Figure 5: Process of activation of p38 $\alpha$  and the biological response after its activation<sup>32</sup>.**

## 6. p38 $\alpha$ MAPK Docking Recruitment Site (DRS)

To understand how p38 $\alpha$  interacts in a molecular level it is necessary to have knowledge of its structure and specifically of its active sites. There is a specific site in the C-terminal lobe of MAP Kinases, known as the D-, KIM-motif (kinase interaction motif), or DRS (docking recognition site), that works as a docking site<sup>5, 33</sup>. The location of the DRS is outside of the active site, and it is different from the DC domain also implicated in docking interactions<sup>34</sup>. The DRS site recognizes a conserved 13-16 amino acid sequence; (R/K)2-3-X2-6- $\Phi$ A-X- $\Phi$ B, where  $\Phi$  is any hydrophobic residue<sup>33</sup>. This amino acid sequence interacts with the DRS groove, that it has four hydrophobic pockets:  $\Phi$ A,  $\Phi$ B,  $\Phi$ L,  $\Phi$ U, and two electrostatic interaction sites  $\Psi$ L, and  $\Psi$ U (also known as the CD site)<sup>35</sup>. Nevertheless, not all the pockets interact at the same time. Depending on the peptide, some pockets will interact, and others will not be necessary for docking. In figure 6, the DRS site in p38 $\alpha$  can be observed along with its pockets.

Many proteins or peptides can bind to the DRS such as activating kinases (MEK2, MKK5, MKK6, MKK3b, STE7), deactivating phosphatases (HePTP, Msg5, DUSP10/MKP5) and substrates/scaffolds (DCC, MEF2a, TAB1, JIP1, NFAT2, SAB, AFT2, Far1, PEA15, RSK1, MNK1, MK2)<sup>5</sup>. However, there should be specific features of the DRS site of p38 $\alpha$  that make it recognizable among MAP kinases. Studies have shown that the residues inside and outside of the DRS domain have a key role in docking and in specificity<sup>36 37</sup>. In addition, peptides can dock to p38 $\alpha$  bidirectionally (C to N, or N to C)<sup>38</sup>. Both, the residues of the DRS and the direction of binding, contribute to the charge and distance between the pockets and make the DRS site of p38 $\alpha$  different among MAP kinases<sup>39</sup>.

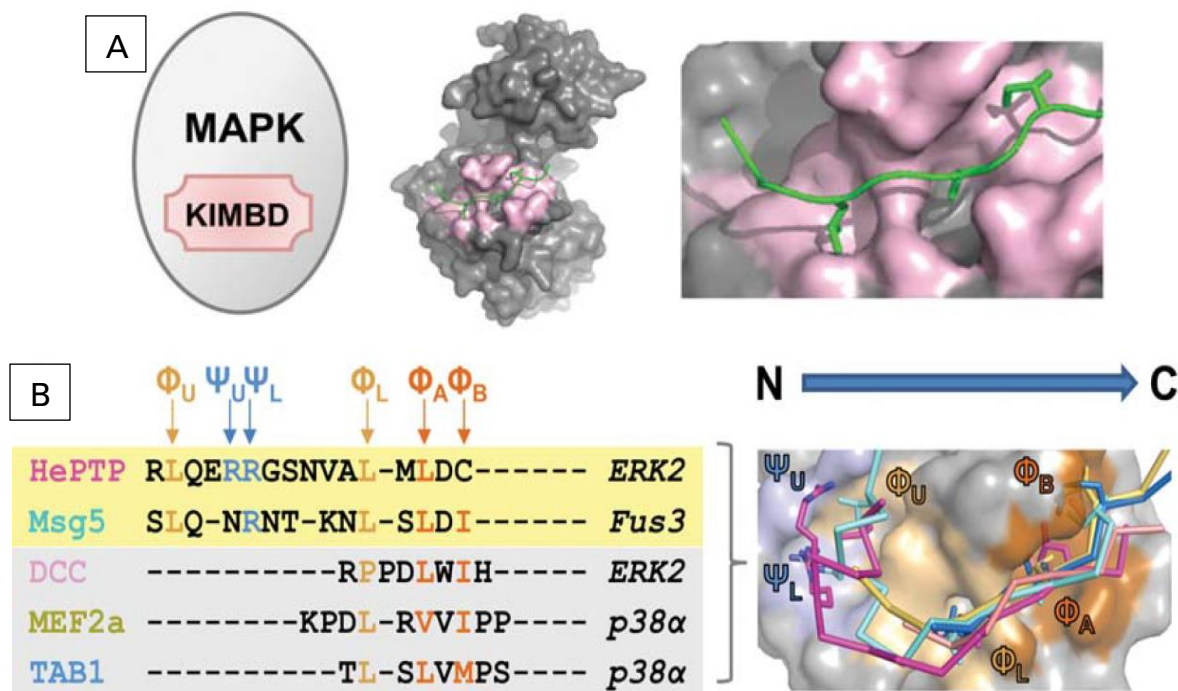


**Figure 6: (A) DRS site (pink) in p38 $\alpha$  and the MEF2A KIM peptide (green). (B) Pockets of the DRS site in ERK2, Fus3, and p38 $\alpha$ . The image is also showing the most common substrates of each enzyme and the scaffold that interacts with the pockets in the DRS<sup>5</sup>.**

## 7. Rooperol

Rooperol is the aglycone of the hypoxoside, a natural compound obtained from the African potato (*Hypoxis hemerocallidea* Lam)<sup>40</sup>. This plant has been used in the Southern part of Africa to heal a variety of diseases such as urinary tract infections, common cold, flu, nausea, and prostate hypertrophy<sup>41, 42</sup>. In addition, studies have shown that the corm polar extracts of *Hypoxis* have antioxidant, antidiabetic, anticonvulsant, antibacterial, antidiarrhoeal, and immunomodulatory properties<sup>43 44</sup>. There are many compounds in the extracts of the African potato, nevertheless, hypoxoside and its aglycone rooperol, are the compounds associated to the medicinal properties of this plant<sup>40</sup>. The structure of the hypoxoside consist of a diphenyl-1-en-4-yne-pentane backbone flanked by two  $\beta$ -D-glucopyranosyl groups<sup>45</sup>. This molecule is

not biologically active but upon hydrolysis rooperol is obtained which is active <sup>46</sup>. The name of the chemical structure of rooperol is ((*E*)-1,5-bis(3',4'-dihydroxyphenyl) pent-1-en-4-yne), and its structure can be observed in figure 7.

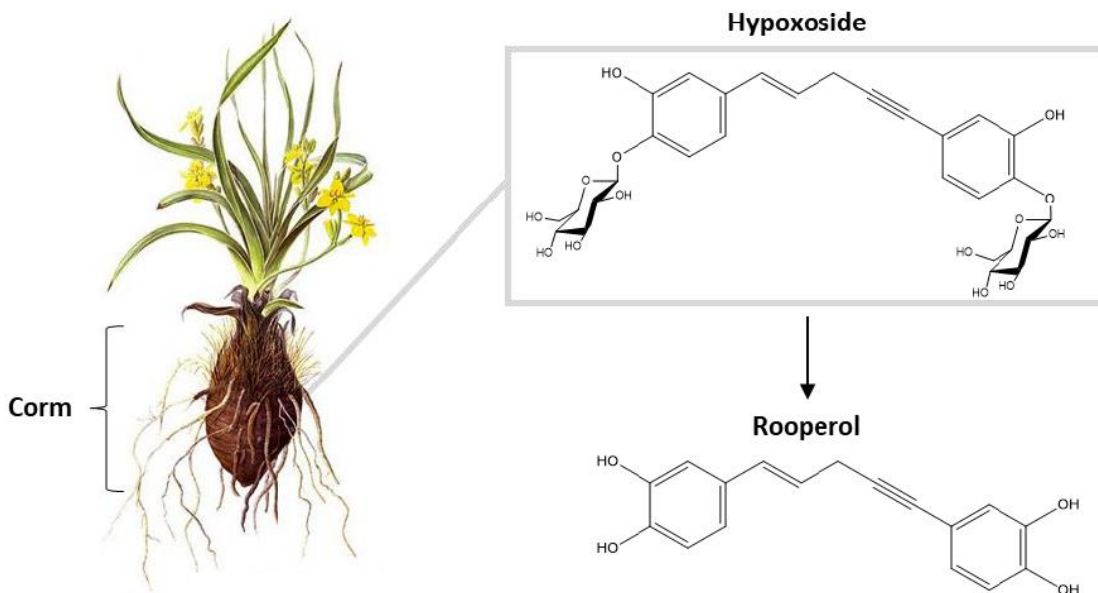
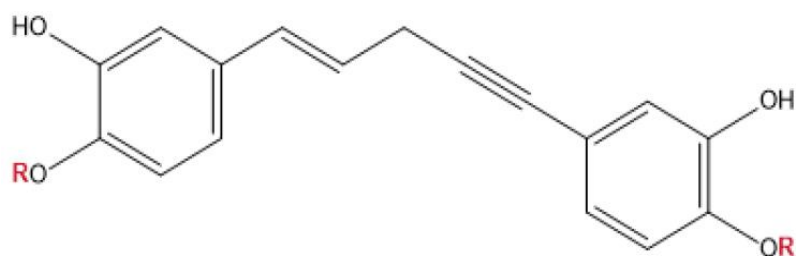


**Figure 7: The African potato and the chemical structure of hypoxoside and rooperol.**

## 8. Metabolism and Activity of Rooperol

Studies has shown that the hypoxoside from the African potato is transformed to rooperol in the colon of mice by bacterial beta-glucosidase <sup>46 45</sup>. Nevertheless, in this species, the hypoxide and rooperol are fast metabolized and converted to sulfates and glucuronides (figure 8) that appear in the portal blood and in the bile <sup>46</sup>. In contrast, in humans, rooperol and its predecessor, can reach relative high concentrations in the serum after oral ingestion of hypoxoside <sup>46</sup> although the T1/2 is low with only 0.55-4.0m <sup>47</sup>. In a phase 1 clinic trial study, it was proved that rooperol is readily converted to phase II

metabolites such as sulfates and glucuronides, the majority of which is a mixed sulfate/glucuronide<sup>48</sup>. Such metabolites of rooperol are eliminated in the urine and are inactive. However, it is important to highlight that a fraction of them, before they are eliminated, can be transformed back to rooperol by beta-glucosidase<sup>46</sup>. In addition, in the phase I clinical study mentioned previously was found that hypoxoside can work as a prodrug without displaying toxicity even at high concentrations (daily dose of 2,400 mg)<sup>48</sup>.



### Phase II Metabolites

R, R' = SO <sub>3</sub> <sup>-</sup> /Glucuronic acid (major)
R=R' = Glucuronic acid (minor)
R=R' = SO <sub>3</sub> <sup>-</sup> (minor)

**Figure 8: rooperol and phase II metabolites.**

Several studies have shown that rooperol can inhibit growth in various cancer cell lines such as B16, HeLa, HT-29, and MCF-7<sup>49 50</sup>. The mechanisms that rooperol follow to inhibit growth in such cells it is not well understood. Some studies claimed that rooperol arrests the cell cycle at late G1 or early S phase, which causes cell apoptosis<sup>50</sup>. A recent study has shown that rooperol inhibit the activity of p38α<sup>51</sup>. Such finding implies that the cytotoxicity of rooperol is due to disruption of the cascades of reactions

between MAPK. A preliminary study by Mooberry, et al. at UT Health Science at San Antonio (unpublished) showed that rooperol causes microtubule depolymerization obstructing replication of cancer cells. Thus, taking in account the findings of all the studies above mentioned, it is probable that the rooperol activity follows many pathways.

## **9. Rooperol and Analogues**

Due to the low stability of rooperol there is an increasing necessity of finding analogues of rooperol with longer T<sub>1/2</sub>. One way to increase the T<sub>1/2</sub> of rooperol is by lowering its propensity to undergo phase II metabolism. This can be attained by synthetically replacing certain metabolically labile groups with alternative groups, in other words, the preparation of an analogue. The choice of analogues usually is done by using bioisosteres. A bioisostere is a substituent group that has similar chemical and physical characteristics and thus may have comparable biological activities to the original group<sup>52</sup>. In the case of rooperol, the aim is to exchange the metabolically labile groups (the two catechols: 3,4-dihydroxybenzene) to avoid the generation of phase II metabolites. Luckily, by changing such groups from rooperol not only the stability but the bioactivity of the molecule could be improved. In a previous study, the hydroxyl groups of the catechols of rooperol were replaced with methyl groups but this analogue showed no activity against several cancer cell lines<sup>42</sup>. Thus, the analogues of rooperol should contain hydroxyl groups. Studies has shown that a good substitute of hydroxyl groups could be fluorine. This atom can increase stability and activity when placed where a hydroxyl group previously was<sup>53</sup>. In our research group there have been prepared analogues of rooperol with bioisosteric replacement of the catechols<sup>54</sup>. Some of the

rooperol analogues proposed by our team contemplates both symmetrical and asymmetrical replacements of the two catechols. Figure 9 shows some of the rooperol analogues synthesized by our Team.

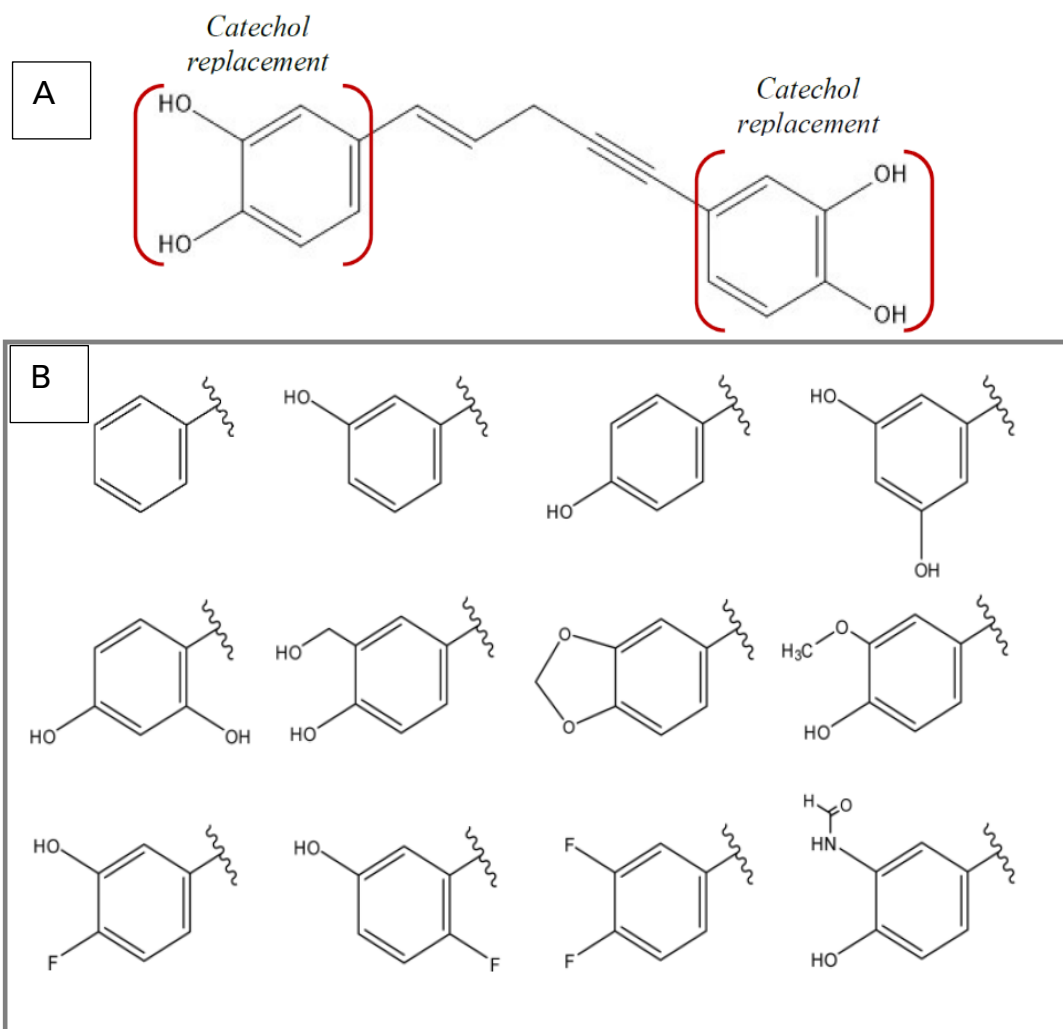


**Figure 9: Rooperol analogues.** (A) rooperol molecule and within brackets the two catechols. (B) Bioisosteric replacements of the two catechols.

## **10. Protein Kinase Docking Approaches in Virtual Screening and Inhibitor Characterization**

Virtual Screening (VS) is a computational way to identify hits and optimized drug leads using computational modeling<sup>55</sup>. VS has its advantages and disadvantages, and it is better to think about it as a complementary technique to High Throughput Screening (HTS). VS required previous knowledge of the structure of the molecules, their energies, and the criteria responsible for binding with a particular target<sup>56</sup>. 3D models of the targeted molecules play a key role in VS to generate a great amount of data about the binding interactions of the system. Through VS it is possible to select or develop hits candidates, to obtain solvation or desolvation information, and more<sup>56</sup>. The basic requirements for VS are:

- A compound collection or library (druglike small molecules)
- The structure of the biological target (protein 3D models)
- An appropriate docking/scoring scheme (docking program)

VS often starts with a series of filter programs that proves the drug-likeness of a library of compounds<sup>57</sup>. This is followed by more complex techniques such as 3D pharmacophore searching, and molecular docking and scoring<sup>58, 59</sup>. In general, there are two approaches in VS; ligand-based virtual screening (LVS) and Structure-based virtual screening (SVS)<sup>60</sup>. The difference between LVS and SVS is that in SVS there is a 3D model of the targeted structure, while in LVS there is not and the LVS is carried out using a ligand (that interact with the targeted molecule) as a base to screen different compounds. SVS usually involves docking molecule libraries to the active site of the

target protein<sup>60</sup>. Then, the pose between the protein with each molecule is scored using a program that predicts the binding free energy<sup>61</sup>. Nowadays, there are more than 60 docking programs available to be used for academic and commercial purposes such as DOCK, AutoDock, FlexX, Surflex, GOLD, ICM, Glide, Cdocker, LigandFit, MCDock, FRED, MOE-Dock, LeDock, AutoDock Vina, rDock, UCSF Dock, and many others<sup>62</sup>.

Protein kinases have become an important area in computational modeling. Just in 2017 there were 620 human protein kinase verified gene sequences<sup>12</sup> and nowadays, there is a web database (kinase.com) that keep updated all the advances in kinase-related genomics knowledge<sup>63</sup>. In addition, there are many 3D protein structure databases available on line such as KLIFS database<sup>64</sup> in which there are more than five thousand PDB structures of kinases. Most of the SVS studies in kinases are conducted with rigid models that do not take in account the flexibility of the molecule due to time saving reasons<sup>12</sup>. However, in a study made by Tian, *et al.* a methodology to investigate kinases by SVS is proposed taking in account the flexibility of the receptors. There are many examples of successful SVS in kinases such as the study performed by Bajusz D, *et al.* In which a selected inhibitor for Janus Kinase (JAK) is discovered<sup>65</sup>. Other examples include a study performed by Lang C A, *et al.* in which joint pharmacophore space (JPS), ensemble docking and sequential JPS-ensemble docking methods were used to discover LRRK2 inhibitors<sup>66</sup>. Nevertheless, there are some weaknesses in virtual screening for kinases such as: most of the efforts are focused to target the conserved ATP binding site, the computational techniques had not successfully identified allosteric binding sites, and most of the studies does not take in account the binding site flexibility in false positives and negatives<sup>67</sup>.

## 11. Binding Assays for Protein Kinase Ligands

There are many ways to measure protein kinase activity. Protein kinases are enzymes that transfer the  $\gamma$ -phosphate from ATP to a serine, threonine, or tyrosine residues in a substrate protein. Thus, one way to measure kinase activity is by measuring the concentration of the phosphorylated product or the change in concentration of the ATP to ADP <sup>68</sup>. The radioisotope filtration binding assay is the traditional method to measure the formation of phosphorylated protein. In this assay a radioisotope of phosphorous (<sup>32</sup>P or <sup>33</sup>P) is used to label the  $\gamma$ -phosphate of ATP <sup>69</sup>. Then, the movement of this labeled phosphate from the ATP to the substrate protein is measured. Finally, the activity of the kinase enzyme is directly related to the amount of labeled  $\gamma$ -phosphate transferred <sup>68</sup>. This method has great sensitivity and resolution, but it is usually avoided by researchers due to problems related with the management of radioactive materials; radioactive safety, waste disposal, and washing and detection processes <sup>68</sup>. Other methods that allow the measurement of kinase activity and do not involve radioactive material include fluorescence and chemiluminescence. Example of such methods are fluorescence intensity (FI), fluorescence polarization (FP), fluorescence resonance energy transfer (FRET), time-resolved fluorescence (TRF), time-resolved fluorescence resonance energy transfer (TR-FRET), and chemiluminescence. Nonetheless, those methods have their own challenges such as assay development, data analysis, and interpretation <sup>68</sup>. The bigger drawback of luminescence and fluorescence methods is that there are a great quantity of fluorescent and luminescent molecules or compounds that can interfere with the results <sup>70</sup>. In addition, there are other methods that do not rely in luminescence or fluorescence such as: scintillation proximity assay, ELISA, mobility shift assay, and protein binding

assay. The major advantage of these methods is that there is little to no compound interference and there is no labeling necessary <sup>71</sup>. Finally, the selection of the kinase assay should be determined by the objective of the research. For instance, in HTS the objective is to test many compounds with a target kinase. Thus, the assay should be robust, reliable, amenable for HTS and low cost. Good examples of HTS assays are fluorescence and luminescence assay. On the other hand, if the objective of the research is to obtain data about a kinase profile, the characteristics of the assay should be acceptable for all kinases in the panel and immune to interferences. Therefore, some assays for kinase profile are the radioisotope-base filtration <sup>68</sup>.

## 12. Research Aims

The first goal of this project was to define the region(s) of the p38 $\alpha$  DRS that are most likely bound by rooperol. Since rooperol has been proposed as an allosteric inhibitor that targets the DRS binding site, it was necessary to test and define the regions of the DRS and its surroundings that are involved in the linkage with rooperol. To answer such inquiry a computational 3D modeling was conducted in which a groove close to the DRS was analyzed using the software Autodock Vina. It is important to highlight that in this work we hypothesized that rooperol's inhibition of p38-alpha will manifest a substrate-specific inhibition, and only p38 $\alpha$  binding partners that are recognized at the DRS will be inhibited by rooperol. In other words, it is possible that rooperol inhibits upstream kinases by targeting the DRS which recognizes such enzymes. The second goal in this work was to adapt the universal ATP-Glow kinase assay for use on a pipetting robot to determine protein kinase inhibition. Therefore, we hypothesize that an automated, universal kinase assay can be developed to determine the inhibitory effects of rooperol and rooperol analogs with specific p38 $\alpha$  MAPK binding partners. To fulfill this goal a kinase assay called ADP-Glow was adapted, minimized, and standardized using a pipetting robot system.

## II. EXPERIMENTAL

### 1. Materials & Instruments

TRIS UltraPure was purchased from VWR, hydrogen peroxide from VWR, 3-aminophthalhydrazine (luminol) from Acros Organics, 4-iodophenylboronic acid (4IPBA) from Acros Organics, DMSO from Fisher Scientific, horseradish peroxidase from MP Biomedicals, MgCl<sub>2</sub> from Fisher Scientific, BSA from Sigma-Aldrich, DTT from Sigma-Aldrich, ADP-Glow™ kit (ultrapure ATP and ADP, ADP-Glow, and Kinase detector) from Promega, MBP from Sigma-Aldrich, staurosporine from Alfa Aesar, p38 $\alpha$  from Abnova, hexokinase from Sigma-Aldrich and syringe filters from VWR.

All aqueous solutions were prepared with water from a Thermo Scientific Barnstead MicroPure Water Purification System. Other instruments used for this project include a pipetting robot model OT-2 from Opentrons, a molecular imager ChemiDoc™ XRS+ Imagine System model Universal Hood II from Bio-Rad Laboratories, a plate reader SpectraMax M3 model MT05905 from Molecular Devices, an Analogue vortex mixer from VWR, and a plate centrifuge PlateFuge from Benchmark.

Coordinate p38 $\alpha$  files were downloaded from the protein data bank (rcsb.org). The structures of p38 $\alpha$  were 1LEW<sup>34</sup>, 2Y80<sup>39</sup>, 2OZA<sup>38</sup>, 2ONL<sup>72</sup>, 2OKR<sup>72</sup>, 2LGC<sup>73</sup>, 1A9U<sup>74</sup>, 3TG1<sup>75</sup>, and 5UOJ<sup>19</sup>. The software used was Autodock Tools from MGL Tools, 1.5.7, Autodock Vina 1.1.2, UCSF Chimera 1.14, and ChemDraw Prime 17.1 from Perkin Elmer Informatics.

## 2. Computational 3D Modeling

To get better understanding of the location, pose and binding energy of rooperol to p38 $\alpha$ , a groove close to the DRS site of the enzyme was analyzed in this work. For practical purposes we called this groove as the alternative groove, and it was analyzed as a complementary study to understand better the binding characteristics of the surroundings of the DRS site.

### 2.1. Methodology

Rooperol was drawn using ChemDraw. Then the structure of the molecule was converted to a 3D file using SMILES line structure building in Chimera. Also in Chimera, the structure was minimized using GAFF force field, and saved as a mol2 file. To compare all the structures of p38 $\alpha$ , all the p38 $\alpha$  PDB files were superimposed with the structure of 1LEW using Chimera mm command. Then all were orientated in the same direction. Thus, the same box could be used for all of them. After that, another preparation was made using AutoDock Tools. In this case the enzyme PDB files were prepared by removing water molecules, adding polar hydrogens, removing non-bonded atoms, and removing any ligand or replicate protein chain. Then, the enzyme was selected as macromolecule for grid and saved as a PDBQT file. Using the Grid Box function of the AutoDock Tools, the grid box was put in the place of the alternative groove in the enzyme structures. The coordinates of the center of the grid box were x center: 35.529, y center: 33.889, and z center: 8.965. The size was 16 in x, 20 in y and 16 in z. Once the p38 $\alpha$  molecules and rooperol were prepared, the next step was to create a run file using a text editor, in which the ligand and the protein were denoted, the box

center location, the size of the box, and exhaustiveness in 32. Then the docking was run with AutoDock Vina obtaining as a result two files: PDBQT and OUT. The PDBQT contains locations and poses of the structures. The OUT file contains the pose, the affinity (kcal/mol), and the RMSD values (root mean square deviation). Then, opening both files in Chimera, the results were visualized.

### **3. Horseradish Peroxidase Assay**

To investigate the two goals of this project, an assay called ADP-Glow™ was standardized using a pipetting robot. The first step in the standardization was to measure the accuracy of the instruments to read the results: a plate reader against a chemidoc. For that reason, an assay that uses horseradish peroxidase enzyme (HRP) was utilized to compare both instruments. This assay was divided in different parts. In the first part, a procedure was developed to find a concentration of HRP measurable in the plate reader as well in the chemidoc. The objective of the second part was to compare accuracy from both equipments at a fixed quantity of HRP. In the third part the signal to noise (S/N) of the two instruments was measured. After the HRP reaction was standardized in the first, second and third part, the aim of the fourth part was to compare the different modes of dispensing of the pipetting robot and choose those that produce the least error.

#### *3.1. Preparation of Stock Solutions*

Six stock solutions were prepared: a buffer, a hydrogen peroxide solution, a luminol solution, an enhancer solution, a juice solution, and the HRP solution. 50 mL of stock buffer solution were prepared using Tris at a concentration of 100 mM. Before

bringing the solution to the desired volume, the pH was adjusted to 8.8 using a solution of HCl 4 M and a solution of NaOH 1 M. To prepare a solution of hydrogen peroxide (10.4 mM), 46  $\mu$ L of 30% hydrogen peroxide were added to 39 mL of buffer tris 100 mM. The luminol solution (1 mL of 250 mM of luminol) was made by adding 44 mg of luminol in 1 mL of DMSO. The enhancer solution (1 mL of 80 mM of 4IPBA) was prepared by adding 20 mg of 4IPBA to 1 mL DMSO. The concentration of the “juice solution” was 5 mM luminol, 800  $\mu$ M 4IPBA, and 5.2 mM H<sub>2</sub>O<sub>2</sub>. 1 mL of this solution was prepared immediately before use by mixing 20  $\mu$ L of luminol (250 mM in DMSO), 10  $\mu$ L of enhancer (80 mM in DMSO), 500  $\mu$ L of peroxide (10.4 mM in buffer Tris 100 mM), and 470  $\mu$ L of buffer Tris (100 mM). Finally, a HRP stock solution of 1 U/10  $\mu$ L was prepared by mixing 2.6 mL of buffer Tris (100 mM) and 1 mg of HRP enzyme (ca. 259 units). The second HRP stock solution (5 mU/10  $\mu$ L) was prepared by mixing 5  $\mu$ L stock HRP enzyme (1 U/10  $\mu$ L) in 995  $\mu$ L of buffer tris.

For the second part of the HRP enzyme assay an extra stock solution of HRP was added. The concentration of this stock solution was 0.31 mU/10  $\mu$ L and was obtained by mixing 62  $\mu$ L stock HRP enzyme (5 mU/10  $\mu$ L) in 938  $\mu$ L buffer tris (100 mM). No other solutions were prepared for the rest of the HRP assay.

### 3.2. *Standard Curves*

The first step to compare instruments using the HRP assay was to choose a concentration of the enzyme that showed signal stability for a long period of time (30 to 60 min). A procedure initially designed for a 96 wells plate<sup>76</sup> was adapted for a 384 wells plate. Then, a protocol for the pipetting robot was built using the Protocol Designer Beta

software offered by the robot’s manufacturer; Opentrons. Such software is available online in the Opentrons webpage <sup>77</sup>. The summary of the robot’s protocol was a) The enzyme dilutions were pipetted in the plate. b) A stop step was programed to allow removal, shaking, and spinning of the plate for 1 min. c) 20 uL of juice solution was pipetted to the enzyme dilutions made in a). d) Another stop step was programed to allow for shaking and spinning the plate for 1 min. Finally, g) The plate was read at different times for a period of one hour. The HRP enzyme dilutions from step a) were obtained as follows: 20 μL of Tris buffer were pipetted in wells “2 through 10”. Then, 40 μL of stock HRP enzyme solution (ca. 5 mU/10 μL) were dispensed in well “1”. Next, 20 μL out of well “1” were transferred to well “2” and mixed. Finally, 20 μL out of well “2” were transferred to well “3”. This process was repeated for wells 4, 5, 6, 7, 8, 9, and 10 to obtain concentrations from 10 mU to 0.0195 mU of HRP. Table 1 shows the dilutions of HRP. In addition, two negatives were measured, one with no HRP enzyme, and the other with buffer.

**Table 1: HRP enzyme units on the serial dilutions.**

Wells	1	2	3	4	5	6	7	8	9	10	11	12
Total mU	10	5	2.5	1.25	0.625	0.3125	0.156	0.078	0.039	0.0195	0	buffer
Enzyme sol.(μL)	20	20	20	20	20	20	20	20	20	20	0	0
Buffer (μL)	0	20	20	20	20	20	20	20	20	20	0	40

For the second part of the HRP enzyme assay a new protocol for the pipetting robot was built modifying some steps from the previous one. The objective of this protocol was to measure the accuracy of the equipment. Therefore, 20 repetitions of the

HRP at a fixed concentration were measured. The summary of the robot's protocol was a) Pipette 20  $\mu\text{L}$  of stock peroxidase enzyme (0.31 mU/10  $\mu\text{L}$ ) to two rows of 10 wells in the plate. d) Pipette 20  $\mu\text{L}$  of juice solution to the wells with enzyme solution. g) Read at different times for a period of one hour by the plate reader and by the chemidoc to compare accuracy in luminescence measurement of both instruments.

A new protocol was developed for the third part of the HRP assay. This new protocol was meant to measure the S/N of the equipment. Therefore, 20 repetitions of the enzyme and 20 repetitions of the buffer were measured for a period of one hour. The protocol for the robot included the next steps: a) Pipette 40  $\mu\text{L}$  of buffer solution to 20 wells in the plate. b) Pipette 20  $\mu\text{L}$  of stock HRP (0.31mU/10  $\mu\text{L}$ ) to 20 empty wells in the plate. c) Pipette 20  $\mu\text{L}$  of juice solution to the 20 wells with HRP solution. d) Shake and spin the plate for one minute. g) Read the plate with the plate reader and the chemidoc at different times for one hour.

In the fourth part, a very different protocol for the robot was developed. This time the protocol was mean to compare the different robot modes to dispense liquid. The parameters took in account were pre-wet tip, touch tip, tip position, multi-dispense, and mixed volume. Table 2 shows the different dispense modes compared in this study. The summary of the robot's protocol was a) Dispense the HRP (0.31 mU/10  $\mu\text{L}$ ) solution in the plate. b) Add the juice solution to all the wells filled with HRP solution. Table 3 shows the way in which the plate was filled.

**Table 2: Modes to dispense and to aspirate of the pipetting robot.**

Mode		Aspirate	Dispense
HRP solution	1	No pre-wet tip, touch tip, change tip once at start.	Tip position 0.5 mm, touch tip
	2	Pre-wet tip, touch tip, change tip once at start	Tip position 0.5 mm, touch tip
	3	Pre-wet tip, touch tip, multi-dispense	Tip position 0.5 mm, touch tip
	4	Pre-wet tip, touch tip, change tip once at start	Tip position 1.0 mm, touch tip
	5	Pre-wet tip, touch tip, change tip once at start	Tip position 0.5 mm, no touch tip
Juice solution	1	Pre-wet tip, touch tip, change tip once at start	Tip position 0.5 mm, touch tip, mix 40 $\mu$ L x 3 times
	2	Pre-wet tip, touch tip, change tip once at start	Tip position 0.5 mm, touch tip, mix 20 $\mu$ L x 3 times

**Table 3: Way in which the plate was filled in part fourth of the HRP assay.** In black are the modes of dispensing the HRP solution. In red are the modes of dispensing the juice solution.

	2	4	6	8	10	12	14	16	18	20
B	1, 1	1, 1	1, 1	1, 1	1, 1	1, 2	1, 2	1, 2	1, 2	1, 2
D	2, 1	2, 1	2, 1	2, 1	2, 1	2, 2	2, 2	2, 2	2, 2	2, 2
F	3, 1	3, 1	3, 1	3, 1	3, 1	3, 2	3, 2	3, 2	3, 2	3, 2
H	4, 1	4, 1	4, 1	4, 1	4, 1	4, 2	4, 2	4, 2	4, 2	4, 2
J	5, 1	5, 1	5, 1	5, 1	5, 1	5, 2	5, 2	5, 2	5, 2	5, 2

#### 4. Standardization of The ADP-Glow Reaction

The first step in the standardization, adaptation, and miniaturization of the ADP-Glow reaction using the pipetting robot was to reproduce the results obtained by Zegzouti H., *et al*<sup>78</sup>. In such study the protocol of the ADP-Glow assay for various kinases in a 96 well plate was described and validated. The parameter that the authors calculated to

validate their results was the  $Z'$  factor and the value that they obtained was 0.7 or higher. This coefficient reflects the changes in the signal range and its relation with the measurements variation<sup>79</sup>. Such coefficient could hold values ranging from negatives to 1. When  $Z'$  is higher than 0.5 the assay has a large band separation and that is considered an excellent outcome. The meaning of these values is shown in table 4. Therefore, to validate the results obtained in the adaptation, miniaturization, and standardization of the ADP-Glow assay using the pipetting robot, the  $Z'$  parameter was the main reference of this work. Additionally, other two parameters were calculated, signal to noise (S/N) and signal to base line (S/B). The S/N is an expression of the level of confidence in which a sign could be identified as real. The S/B is the ratio of the mean signal divided by the mean background. This factor does not take into account the variations of the measurements, therefore; it does not offer a reliable judgment of the assay<sup>79</sup>. The  $Z'$  factor, S/N, and S/B were calculated as follow:

$$S/N = \frac{\text{Mean signal} - \text{Mean background}}{\text{Standar deviation of background}}$$

$$S/B = \frac{\text{Mean signal}}{\text{Mean background}}$$

$$Z' = \frac{3 \text{ SD of sample} + 3 \text{ SD of control}}{(\text{mean of sample} - \text{mean of control})}$$

**Table 4: meaning of the  $Z'$  values.**

Z factor value	Structure of assay	Related to screening
1	SD=0, (no variation, or the dinamic range is $\infty$ )	an ideal assay
$1 > Z \geq 0.5$	Separation band is large	an excelent assay
$0.5 > Z > 0$	Separation band is small	a double assay
0	No separation band, the sample signal variation and control signal variation bands touch.	A yes/no type of assay
< 0	No separation band, the sample signal variation and control signal variation bands overlap.	Screening virtually imposible.

It is important to highlight that the miniaturization of the assay in this work meant that the ADP-Glow was adapted from the original reaction, which was held in a 96 well plate, to a reaction carried out into a 384 well plate. Thus, the volumes of the reactants were significantly reduced. In addition, this reaction was adapted and standardized to be used in a pipetting robot.

During the first attempt to reproduce the results from the article of Zegzouti H and coworkers in a miniaturized way using the pipetting robot, the points below 10% of ADP conversion did not fall into linear tendency. Therefore, it was necessary to obtain higher accuracy for these points. Thus, for the second attempt to reproduce the Zegzouti H results, a modified procedure was developed. Once an acceptable ATP-ADP conversion curve was obtained, the second step was to measure the effect of the solvent, DMSO, in the reaction. This step was necessary because in next steps the inhibitor is diluted in DMSO. The third step was to make a new correction to the ATP-ADP percent conversion curve. In previous steps the concentration of the ATP was at a fixed concentration instead of diminishing as the ADP increased. Thus, the pertinent adjustments to obtain a conversion curve with the desired concentrations of ATP and ADP for each point of the curve were made. The fourth step was to test the p38 $\alpha$  enzyme using the pipetting robot and to find an adequate concentration of the enzyme. The fifth step was to find a concentration of the substrate, myelin, that produced more luminescence than the luminescence obtained in the previous step. The sixth step and final step was to adapt the procedure suggested by Promega<sup>80</sup>, to titrate p38 $\alpha$  using staurosporine as inhibitor.

#### 4.1. Preparation of Stock Solutions

The ADP-Glow reaction involves two curves, the ATP-ADP conversion curve, and the kinase curve. The volumes used in the wells for the ATP-ADP conversion curve were 5  $\mu\text{L}$  of ATP-ADP solution, 5  $\mu\text{L}$  of ADP-glow reagent and 10  $\mu\text{L}$  of kinase detector reagent. For the kinase curve, 2  $\mu\text{L}$  of substrate solution, 3  $\mu\text{L}$  of kinase solution, 5  $\mu\text{L}$  of ADP-glow reagent, and 10  $\mu\text{L}$  of kinase detector reagent were used. Also, a final concentration in the plate (10  $\mu\text{M}$  of ATP) 10 times smaller than the concentration suggested in the paper from Zegzouti H was used in this experiment. This concentration was tested to have higher accuracy at low concentrations of ATP.

Nine stock solutions were prepared for the first attempt to reproduce the Zegzouti H results at a concentration of 10  $\mu\text{M}$ . These solutions were buffer A 1X, 100  $\mu\text{M}$  ADP, 100  $\mu\text{M}$  ATP, 10  $\mu\text{M}$  ATP, 10  $\mu\text{M}$  ADP, hexokinase solution, 250 mM dextrose, 2.5 mM dextrose, and Substrate solution (a solution made by dextrose, ATP, and buffer). The composition of the buffer A 1X was 40 mM of Tris (pH 7.5), 20 mM of  $\text{MgCl}_2$ , and 0.1 mg/mL of BSA. The procedure to obtain the buffer was to add 0.2422 g of Tris and 0.2035 g of  $\text{MgCl}_2$  to 35 mL of MiliQ water. Once the salts were dissolved the pH was adjusted to 7.5 using a solution of NaOH 4 M and a solution of HCl 1 M. Then, 5 mg of BSA were added, and the volume was brought to 50 mL. Finally, the buffer was sterilized using a syringe filter. The ADP and ATP 100  $\mu\text{M}$  solutions were prepared by mixing 5  $\mu\text{L}$  of 10 mM ultrapure ADP or ATP in 495  $\mu\text{L}$  of buffer A 1X. The 10  $\mu\text{M}$  ATP was obtained by mixing 100  $\mu\text{L}$  of ATP 100  $\mu\text{M}$  with 900  $\mu\text{L}$  of buffer A 1X. The same procedure was applied to obtain the 10  $\mu\text{M}$  ADP. The hexokinase solution (0.033 U/ $\mu\text{L}$ ) was prepared by dissolving 0.00013 g of hexokinase in 906  $\mu\text{L}$  buffer A 1X. The

dextrose 250 mM was prepared by dissolving 0.495 g of dextrose in 10 mL of MiliQ water. Then, the dextrose 2.5 mM was prepared by diluting 100  $\mu$ L of dextrose 250 mM in 9900  $\mu$ L of MiliQ water. Finally, the substrate solution was prepared with both ATP and dextrose at a concentration of 0.025 mM to have a final concentration of 10  $\mu$ M in the wells. Thus, 50  $\mu$ L of ATP 100  $\mu$ M, 2  $\mu$ L of dextrose 2.5 mM, and 148  $\mu$ L of buffer A 1X were mixed. For the second attempt to reproduce the results obtained from Zegzouti H at a concentration of 10  $\mu$ M ATP, the procedure to make the ATP-ADP percentage conversion curve was modified. However, the solutions were the same as the solutions for the first attempt.

For the second step to adapt the ADP-glow reaction to the pipetting robot, a measurement of the effect of the DMSO solvent was performed. To complete this experiment, 11 solutions were made: buffer A 1X, and buffer A 1X +DMSO at 20%, 100  $\mu$ M ADP, 100  $\mu$ M ATP, 10  $\mu$ M ATP, 10  $\mu$ M ADP, hexokinase solution at 0.0066 U/ $\mu$ L and at  $6.6 \times 10^{-5}$  U/ $\mu$ L, 250 mM dextrose, 2.5 mM dextrose, and Substrate solution. The buffer A 1X +DMSO at 20% was made by mixing 200  $\mu$ L of DMSO and 800  $\mu$ L of buffer A 1X to have a total volume of 1mL. The hexokinase solution at 0.0066 U/ $\mu$ L was prepared by diluting 0.05 mg hexokinase in 1742  $\mu$ L of buffer A 1X to have a total volume of 1742  $\mu$ L. The hexokinase solution at  $6.6 \times 10^{-5}$  U/ $\mu$ L was made by mixing 10  $\mu$ L of HK at 0.0066 U/ $\mu$ L with 990  $\mu$ L of buffer A 1X to have a total volume of 1 mL. The rest of the solutions were obtained as described in the previous step.

The third step was meant to make a new correction in the ATP-ADP percent conversion curve. At this point in the project, we realized that the ATP in the ATP-ADP curve was at a fixed concentration instead of diminishing as the ADP increased. To solve

that problem a new protocol with 8 solutions was made. Such solutions were buffer A 5X, 100 mM of DTT in water, 4 X Kinase Buffer D, 10X ATP, 10X ADP, 3 mL of 300  $\mu$ M ATP, 800  $\mu$ L of 150  $\mu$ M ATP, and 200  $\mu$ L of 150  $\mu$ M ADP. The buffer A 5X was made following the steps for the buffer A 1X but 5 times more concentrated. The 100 mM of DTT solution was made by dissolving 0.1542 g of DTT in 10 ml of MiliQ water. The concentration of the 4 X Kinase Buffer D was 160 mM Tris [pH 7.5], 80 mM MgCl<sub>2</sub>, 0.4 mg/mL BSA, 200  $\mu$ M DTT, and 4% DMSO. This buffer was made by mixing 40 mL of buffer A 5X with 100  $\mu$ L of 100 mM DTT and 2 mL of DMSO. Then the volume was adjusted to 50 mL with MiliQ water. Then, it was sterilize using a syringe filter. The 10X ATP (1.5 mM) was made by diluting 105  $\mu$ L of 10 mM ultrapure ATP in 595  $\mu$ L of MilliQ water to obtain a total volume of 700  $\mu$ L. The 10X ADP (1.5 mM) was obtain by adding 12  $\mu$ L of 10 mM ultrapure ADP to 68  $\mu$ L of MilliQ water to have a total volume of 80  $\mu$ L. The 3 mL of 300  $\mu$ M ATP were made by mixing 600  $\mu$ L of 10X ATP, 750  $\mu$ L of 4x Kinase Buffer D, and 1650  $\mu$ L of MilliQ water. The 800  $\mu$ L of 150  $\mu$ M ATP were made by mixing 80  $\mu$ L of 10X ATP, 200  $\mu$ L of 4x Kinase Buffer D, and 520  $\mu$ L of MilliQ water. Finally, the 200  $\mu$ L of 150  $\mu$ M ADP were made by mixing 20  $\mu$ L of 10X ADP, 50  $\mu$ L of 4x Kinase buffer D, and 130  $\mu$ L of MiliQ water.

The fourth step was meant to test p38 $\alpha$  with myelin as a substrate. To perform this experiment 12 solutions were made: buffer A 1X, 100 mM of DTT, 4X Kinase Buffer D, 10X ATP, 10X ADP, 3 mL of 300  $\mu$ M ATP, 800  $\mu$ L of 150  $\mu$ M ATP, 200  $\mu$ L of 150  $\mu$ M ADP, p38 $\alpha$  kinase 10 ng/ $\mu$ L, MBP solution, Substrate solution, and 400  $\mu$ L of 1X Kinase buffer D. The 20  $\mu$ L of p38 $\alpha$  kinase (10 ng/ $\mu$ L) were made by mixing 1  $\mu$ L of 200 ng/ $\mu$ L of p38 $\alpha$  stock enzyme, 5  $\mu$ L of 4X Kinase buffer D, and 14  $\mu$ L of MilliQ water. The

MBP stock solution (1 mg/mL) was made by adding 1 mL of MilliQ water to the stock powder of myelin basic protein (1 mg). The concentration of the Substrate solution was 0.25 mg/ml of MBP and 2.5X ATP (375  $\mu$ M). This solution was made by mixing 50  $\mu$ L of 10X ATP, 50  $\mu$ L of 4X Kinase buffer D, 50  $\mu$ L of MilliQ water, and 50  $\mu$ L MBP (1 mg/mL). The rest of the solutions were obtained as previously described in the third step.

In the fifth step, different concentrations of MBP were tested to find at which concentration the enzyme p38 $\alpha$  was capable to produce more luminescence. For this step only two solutions were made different, one was new, and the rest of the solutions were prepared in the same way as in the fourth step. The Substrate solution for this experiment was prepared at a concentration of 0.5 mg/ml of MBP and 2.5X ATP (375  $\mu$ M). To obtain such concentration 50  $\mu$ L of 10X ATP, 50  $\mu$ L of 4X Kinase Buffer D, and 100  $\mu$ L of MBP (1 mg/mL) were mixed to obtain a final volume of 200  $\mu$ L. The solution of p38 $\alpha$  kinase (10 ng/ $\mu$ L) was prepared by adding 3  $\mu$ L of the stock enzyme (200 ng/ $\mu$ L), 15  $\mu$ L of 4X Kinase Buffer D, and 42  $\mu$ L of MilliQ water to obtain a final volume of 60  $\mu$ L. The 200  $\mu$ L of 375  $\mu$ M ATP were prepared by mixing 50  $\mu$ L of 4X Kinase Buffer D, 50  $\mu$ L of 10X ATP, and 100  $\mu$ L MilliQ water.

The objective of the sixth step was to adapt the procedure suggested by Promega<sup>80</sup>, to titrate p38 $\alpha$  with staurosporine as inhibitor using the pipetting robot. For this step, 15 different solutions were made: buffer A 1X, 100 mM of DTT, 4 X Kinase Buffer D, MBP solution (1 mg/mL), staurosporin stock solution (10,000  $\mu$ M), 10X ATP, 10X ADP, 3 mL of 300  $\mu$ M ATP, 800  $\mu$ L of 150  $\mu$ M ATP, 200  $\mu$ L of 150  $\mu$ M ADP, Substrate solution (0.5 mg/ml of MBP, 2.5X ATP (375  $\mu$ M)), p38 $\alpha$  kinase solution (10 ng/ $\mu$ L), 100  $\mu$ L of 500  $\mu$ M staurosporin, and 1X Kinase Buffer D in 1% DMSO. Most of

the solutions were prepared exactly as previously described in steps fifth, and fourth. Therefore, only changed, and new solutions are described in this step. The staurosporin solution (10,000  $\mu\text{M}$ ) was prepared by adding 214  $\mu\text{L}$  DMSO to the stock staurosporin powder of 1 mg. The 100  $\mu\text{L}$  of 500  $\mu\text{M}$  staurosporin were prepared by mixing 70  $\mu\text{L}$  of MiliQ water, 25  $\mu\text{L}$  of 4X Kinase Buffer D, and 5  $\mu\text{L}$  staurosporine stock solution (10,000  $\mu\text{M}$ ). The 1X Kinase Buffer D in 1% DMSO solution was prepared by diluting 250  $\mu\text{L}$  of 4X Kinase Buffer D in 750  $\mu\text{L}$  of MiliQ water.

#### 4.2. *Standard Curves*

In the first attempt to reproduce the procedure from Zegzouti H, a protocol for the pipetting robot was built using the Protocol Designer Beta software offered by the robot's manufacturer; Opentrons. Such protocol contemplated the next steps; a) Pipetting buffer A 1X for the HK dilutions. b) Pipetting the ADP for the curve. c) The robot was programmed to pause to allow the removal of the plate to centrifuge it 60 seconds. d) The HK dilutions were pipetted. e) The ATP was pipetted in the wells filled with ADP to obtain the conversion curve. f) The robot was programmed to pause again to allow the removal of the plate to shake and centrifuge it 60 seconds. g) The HK points were pipetted into the plate. h) The robot was paused to allow the removal of the plate to centrifuge it 60 seconds. i) The Substrate solution was pipetted to the wells filled with the HK points. j) The robot was paused 30 mins to allow the removal of the plate for shaking and centrifuging it, and to allow the reaction between the hexokinase and the Substrate solution. k) The repetitions of the ATP-ADP curve were pipetted while waiting for the reaction between HK and substrate solution. l) The robot was paused to centrifuge the

plate. m) Once the reaction between the HK and the Substrate solution was ended, the ADP-Glow was pipetted. n) The robot was paused to shake and centrifuge the plate for 60 seconds, then it was incubated 40 mins in absence of light. o) The kinase detection reagent was added to each well. p) The plate was shaken and centrifuged for 60 seconds one last time. q) The plate was incubated 60 minutes in absence of light. r) The plate was read at 30 mins incubation, placed back into darkness, and read again at 60 mins of incubation. The two readings were performed by the plate reader. The percent ATP-ADP conversion curve pipetted in steps b) and e) were made according to table 5. The hexokinase dilutions (10-fold dilutions; 10  $\mu$ L of HK dilution in 90  $\mu$ L buffer A 1X) have the concentrations displayed in table 6.

**Table 5: ATP-ADP conversion curve (first attempt).**

%	ADP ( $\mu$ L)	ATP ( $\mu$ L)
0	-	100
1	1	99
2	2	98
4	4	96
5	5	95
10	10	90
20	20	80
40	40	60
80	80	20
100	100	-

**Table 6: Concentrations of HK dilutions.**

Concentration mU/ $\mu$ L	mU in 3 $\mu$ L
3.300	10.00
0.330	1.000
0.033	0.100
0.003	0.010
0.0003	0.001

For the second attempt, the protocol for the robot was optimized in time by organizing the steps. The summary of the robot's procedure was a) Pipetting the HK dilutions in the plate. b) The robot was programmed to pause to allow the removal of the plate to shake and centrifuge it 60 seconds. c) The HK repetitions were pipetted. d) The substrate solution was pipetted into the HK repetitions. d) The robot was paused to allow the removal of the plate to shake and centrifuge it 60 seconds. A timer was set for 40 min. e) The points for the ATP-ADP curve were pipetted in the plate while waiting for the end of the timer. f) The repetitions of the ATP-ADP curve were pipetted while waiting for the end of the timer. g) The robot was paused to shake and centrifuge the plate 60 seconds. h) Once the 40 minutes timer ended, the ADP-Glow reagent was pipetted in all the wells filed with the ATP-ADP curve points and HK points. i) The robot was paused to allow the removal of the plate to shake and to centrifuge it for 60 seconds. j) The plate was incubated 40 mins in the dark. k) The kinase detection reagent was pipetted to each well. l) The plate was shaken and centrifuged 60 seconds. m) The plate was incubated 60 mins in the dark. n) The plate was read at 60 and 30 of mins incubation by a plate reader. The ATP-ADP percentage conversion (step e) curve was built by adding 50  $\mu$ L of stock solution 10  $\mu$ M ATP to nine wells in a plate row (1, 2, 3, 4, ...). Then, 50  $\mu$ L of stock

solution 10  $\mu$ M ADP were added to well 2 and mixed. Then, 50  $\mu$ L were transferred from well 2 to well 3. The liquid in the well 3 was mixed very well. Finally, steps in 2 and 3 were repeated for the rest of the wells to obtain the ATP-ADP percentage conversion points; 100, 50, 25, 12.5, 6.25, 3.125, 1.562, 0.781. The hexokinase concentrations were the same as in the first attempt.

The objective of the second step to adapt the ADP-Glow reaction was to explore the effect of the DMSO in the reaction. To be able to observe the changes produced by such solvent only one concentration of the hexokinase was used (0.1 mU). The ATP-ADP percent conversion curve was obtained as described in the previous step. The summary of the robot's protocol was a) The HK + DMSO dilutions were made in the plate. b) The robot was paused to shake and centrifuge the plate 60 seconds. c) The repetitions of the HK +DMSO dilutions were pipetted. d) The Substrate solution was pipetted into HK +DMSO repetitions. e) The robot was paused to allow the removal of the plate to shake and centrifuge it 60 seconds. A timer for 40 min was set to let the HK and the substrate solution to react. f) The ATP-ADP dilutions were made in the plate while waiting to the end of the 40 minutes timer. g) The ATP-ADP repetitions were pipetted while still waiting the end of the 40 minutes timer. h) The robot was paused to shake and centrifuge the plate 60 seconds. i) Once the 40 minutes ended, the ADP-Glow was pipetted to all the wells. J) The robot was paused to allow the removal of the plate to shake and centrifuge it 60 seconds. k) The plate was incubated 40 mins in light absence. l) The kinase detection reagent was pipetted to each well. m) The plate was shaken and centrifuged 60 seconds, n) The plate was incubated 60 mins in absence of light. o) Finally, the plate was measured at 30 mins incubation and at 60 mins incubation by a

plate reader.

The Hexokinase + DMSO dilutions were obtained by making a serial dilution 1:1 with the HK  $6.6 \times 10^{-5}$  U/ $\mu$ L and the buffer A 1X +DMSO at 20%. To obtain the dilutions 50  $\mu$ L from the HK stock solution was transferred to wells 1, 2, 3, 4, and 5. Then, 50  $\mu$ L from buffer A 1X +DMSO at 20% were transferred to well 1 and mixed very well. Then 50  $\mu$ L were transferred from well 1 to well 2, then 50  $\mu$ L from well 2 to well 3, and so on. Then well 6 was filled with 50  $\mu$ L of HK stock solution + buffer A 1X (without DMSO) to obtain the 0%. Table 7 shows the DMSO concentrations.

**Table 7: DMSO concentrations**

Concentration of DMSO %	HK mU in 3 uL
10.0	0.1
5.00	0.1
2.50	0.1
1.25	0.1
0.63	0.1
0.00	0.1

The new correction to the ATP-ADP percent conversion curve was made as a third step to adapt the ADP-Glow reaction to the use of the pipetting robot. In previous steps the concentration of the ATP was kept constant instead of decreasing as the ADP increased in concentration. To fix the concentration of the ATP, a series of new dilutions of ATP were made in the robot. Table 8 shows the ATP dilutions.

**Table 8: ATP dilutions for correction of ATP-ADP curve.**

ATP Dilution Number	$\mu\text{L}$ of 300 $\mu\text{M}$ ATP	$\mu\text{L}$ of 150 $\mu\text{M}$ ATP	Total volume $\mu\text{L}$
1	250	250	500
2	375	125	500
3	438	62	500
4	469	31	500
5	485	15	500
6	492	8	500

Then, the points for the ATP-ADP percent conversion curve were obtained by making a series of dilutions of 150  $\mu\text{M}$  ADP in the different dilutions of ATP showed in table 8. Table 9 displays the dilutions of ADP in ATP that were done to obtain the corrected conversion curve.

**Table 9: Dilutions of ADP in ATP to obtain the corrected ATP-ADP percent conversion curve.**

%Conversion	%ADP	%ATP	ATP dilution In well	Procedure
100	100	-		150 $\mu\text{M}$ ADP in 1x Kinase Buffer D is the 100%
50	50	50	----	Mix 50 $\mu\text{L}$ of 150 $\mu\text{M}$ ADP + 50 $\mu\text{L}$ of 150 $\mu\text{M}$ ATP in well A1
25	25	75	50 $\mu\text{L}$ #1 in A2	Remove 50 $\mu\text{L}$ from A1 and move to A2, mix
12.5	12.25	87.5	50 $\mu\text{L}$ #2 in A3	Remove 50 $\mu\text{L}$ from A2 and move to A3, mix
6.25	6.25	93.75	50 $\mu\text{L}$ #3 in A4	Remove 50 $\mu\text{L}$ from A3 and move to A4, mix
3.125	3.125	96.87	50 $\mu\text{L}$ #4 in A5	Remove 50 $\mu\text{L}$ from A4 and move to A5, mix
1.56	1.56	98.44	50 $\mu\text{L}$ #5 in A6	Remove 50 $\mu\text{L}$ from A5 and move to A6, mix

0.78	0.78	99.22	50 $\mu$ L #6 in A7	Remove 50 $\mu$ L from A6 and move to A7, mix. Remove 50 $\mu$ L from A7 and discard
0	0	100		150 $\mu$ M ATP in 1x Kinase Buffer D is the 100%

The summary of the robot's protocol was a) The ATP dilutions (table 8) were pipetted on the Eppendorf rack. b) The robot stopped, and Eppendorf tubes were mixed. c) The ATP-ADP curve (Table 9) was pipetted. d) The robot stopped, and the plate was shaken and centrifuged for 60 seconds. e) The ATP-ADP repetitions were pipetted. f) The ADP-Glow was pipetted. g) The robot was paused to allow the removal of the plate to shake and to centrifuge it 60 seconds, then it was incubated 40 mins in absence of light. h) The kinase detection reagent was pipetted, i) The robot was stopped to allow the removal of the plate to shake and to centrifuge it 60 seconds. j) The plate was incubated 60 mins in absence of light. then, it was read at 30 mins and 60 mins of incubation.

The fourth step was to test p38 $\alpha$  using MBP as a substrate. The objective of this step was to find an appropriate concentration of the enzyme. Therefore, different concentrations of the enzyme were obtained by making a serial dilution of 1:1 with the stock p38 $\alpha$  (10 ng/ $\mu$ L) in 1X Kinase Buffer D. Table 10 shows the serial dilutions of p38 $\alpha$ .

**Table 10: Serial dilutions of p38 $\alpha$ .**

Concentration ng/ $\mu$ L	ng in 3 $\mu$ L
10.0	30.0
5.00	15.0
2.50	7.50
1.25	3.75
0.63	1.89
0.31	0.93
0.16	0.48
0.08	0.24
0.04	0.12
0.000	0.00

The summary of the robot's protocol is a) The p38 $\alpha$  dilutions were pipetted in the plate (table 10). b) The robot was programmed to stop to mix and spin the plate 1 min. c) The p38 $\alpha$  duplicates were pipetted in the plate. d) The substrate solution was pipetted to the P38 $\alpha$  duplicates. e) A timer of 40 mins was set to allow the enzyme and the substrate to react. f) In the meantime, the steps for the ATP-ADP conversion curve were performed: the ATP dilutions were pipetted on an Eppendorf rack (table 8). The robot was stopped to mix ATP dilutions. The ATP-ADP curve (Table 9) was pipetted. The ATP-ADP repetitions were pipetted. g) Once the 40 mins finished the ADP-Glow was pipetted to all the wells. h) The robot was paused to allow to remove the plate to shake and centrifuge it 60 seconds. i) The plate was incubated 40 mins in absence of light. j) The kinase detector reagent was pipetted to each well. k) The plate was shaken and centrifuged 60 seconds, then incubated 60 mins in absence of light. l) The plate was read at 30 and 60 mins of incubation.

In the fifth step different concentrations of the MBP substrate were tested. This experiment was necessary because in the previous experiment (step fourth) the enzyme did not show high activity. The concentrations of MBP tested in this experiment were done by the robot and are shown in table 11.

**Table 11: Concentrations of MBP**

% of Substrate Solution	100%	80%	60%	40%	20%	0%
Volume of substrate solution	50 $\mu$ L	40 $\mu$ L	30 $\mu$ L	20 $\mu$ L	10 $\mu$ L	0 $\mu$ L
ATP 375 $\mu$ M in 4x kinase buffer D	0 $\mu$ L	10 $\mu$ L	20 $\mu$ L	30 $\mu$ L	40 $\mu$ L	50 $\mu$ L
Concentration of substrate solution (mg/mL)	0.5	0.4	0.3	0.2	0.1	0.0

The summary of the robot's protocol was a) The MBP dilutions were pipetted in the plate (table 11). b) The robot was programmed to stop, to allow the removal of the plate to mix and spin it 1 min. c) The MBP dilution were pipetted in triplicate. d) p38alpha was pipetted to the MBP triplicates. e) A timer was set for 80 min to allow the reaction between the enzyme and the substrate. f) Meanwhile, the steps for ATP-ADP conversion curve were performed: the ATP dilutions were pipetted on an Eppendorf rack (table 8). The robot was stopped to mix ATP dilutions. The ATP-ADP curve (Table 9) was pipetted. The ATP-ADP repetitions were pipetted. g) Once the 80 mins finished the ADP-Glow was pipetted to all the wells. h) The robot was paused to allow the removal of the plate to shake and centrifuge it 60 seconds. i) The plate was incubated 40 mins in absence of light. j) The kinase detector reagent was pipetted to each well. k) The plate was shaken and centrifuged 60 seconds. Then, it was incubated 60 mins in absence of light. l) The plate was read at 30 and 60 mins of incubation.

The object of the sixth step was to adapt the procedure suggested by Promega, to titrate p38 $\alpha$  with staurosporine using the pipetting robot. Therefore, a series of staurosporine dilutions were prepared. Table 12 shows the different dilutions of staurosporine prepared using the robot.

**Table 12: Staurosporine dilutions.**

Well	Conc. in row P (nM)	Procedure	Final con. (nM)
P1	100000	Transfer 100 $\mu$ L of staurosporine stock solution (100000 nM) to well P1	500000
P2	20000.0	Add 80 $\mu$ L of buffer 1X Kinase buffer D and transfer 20 $\mu$ L from well P1	100000
P3	4000.00	Add 80 $\mu$ L of buffer 1X Kinase buffer D and transfer 20 $\mu$ L from well P2	20000.0
P4	800.000	Add 80 $\mu$ L of buffer 1X Kinase buffer D and transfer 20 $\mu$ L from well P3	4000.00
P5	160.000	Add 80 $\mu$ L of buffer 1X Kinase buffer D and transfer 20 $\mu$ L from well P4	800.000
P6	32.0000	Add 80 $\mu$ L of buffer 1X Kinase buffer D and transfer 20 $\mu$ L from well P5	160.000
P7	6.40000	Add 80 $\mu$ L of buffer 1X Kinase buffer D and transfer 20 $\mu$ L from well P6	32.0000
P8	1.28000	Add 80 $\mu$ L of buffer 1X Kinase buffer D and transfer 20 $\mu$ L from well P7	6.40000
P9	0.25600	Add 80 $\mu$ L of buffer 1X Kinase buffer D and transfer 20 $\mu$ L from well P8	1.28000
P10	0.05120	Add 80 $\mu$ L of buffer 1X Kinase buffer D and transfer 20 $\mu$ L from well P9	0.25600
P11	0.0	Transfer 100 $\mu$ L 1x kinase buffer D to well P11	0.0
P12	0 (No enzyme)	Transfer 100 $\mu$ L 1x kinase buffer D to well P12. p38 $\alpha$ is not added to these repetitions.	0.0

The summary of the robot's protocol was a) The staurosporine dilutions were made in in row P (table 12). b) The robot was programed to stop to mix and spin the plate 1 min. c) Staurosporine dilutions were pipetted in triplicate. d) p38 $\alpha$  was pipetted to the staurosporine triplicates. e) The Substrate solution (0.5 mg/mL) was pipetted in the wells

filled with the reaction. f) A timer was set for 80 min to allow the reaction between the enzyme and the substrate. g) Meanwhile, the steps for ATP-ADP conversion curve were performed: the ATP dilutions were pipetted on an Eppendorf rack (table 8). The robot was stopped to mix ATP dilutions. The ATP-ADP curve (Table 9) was pipetted. The ATP-ADP repetitions were pipetted. h) Once the 80 minutes finished the ADP-Glow was pipetted. i) The robot was paused to allow removal of the plate to shake and centrifuge it 60 seconds. j) The plate was incubated 40 mins in absence of light. k) The kinase detector reagent was pipetted to each well. l) The plate was shaken and centrifuged 60 seconds, then incubated 60 mins in absence of light. m) The plate was read at 30 and 60 mins of incubation.

### III. RESULTS & DISCUSSION

#### 1. Computational 3D Modeling

The first part of these work is the docking of p38 $\alpha$  with rooperol. This part of the project was intended to have a better understanding of the interaction between rooperol and the surroundings of the DRS site in p38 $\alpha$ . In this case a groove close to the DRS site of the enzyme was analyzed, and for practical purposes was called the alternative groove. The coordinates of the box center that corresponds to the alternative groove are x center: 35.529, y center: 33.889, and z center: 8.965. The size was 16 in x, 20 in y and 16 in z. Figure 10 shows the location of the alternative groove and figure 11 shows the locations for the DRS and the alternative groove.

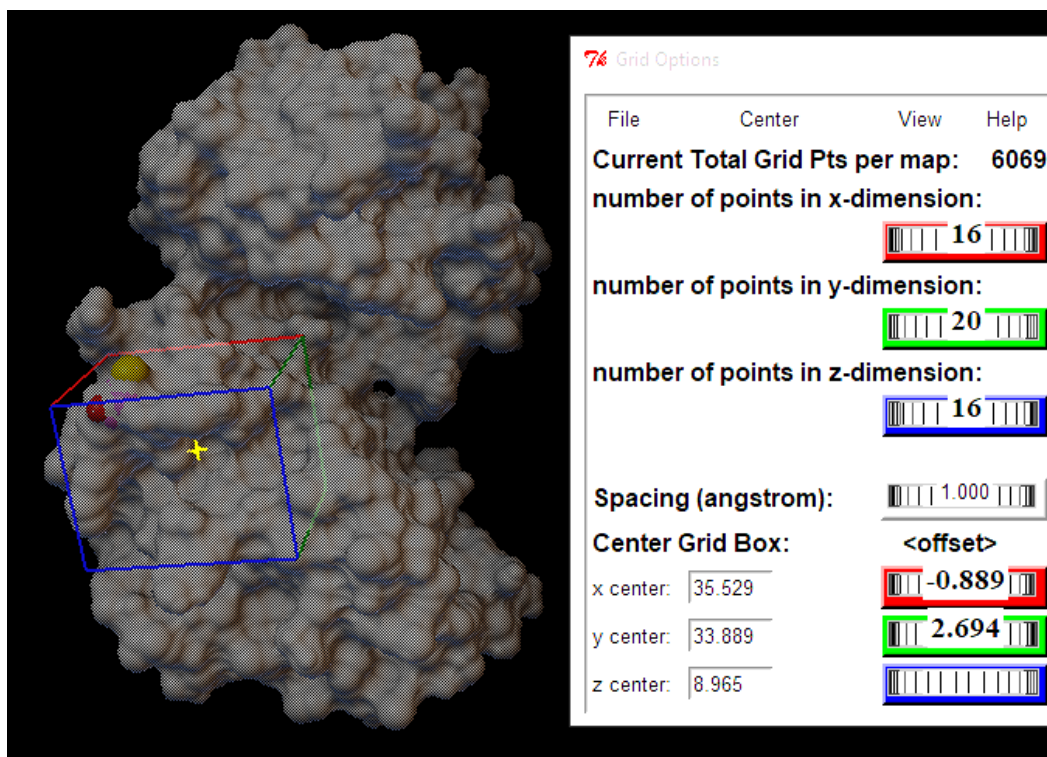
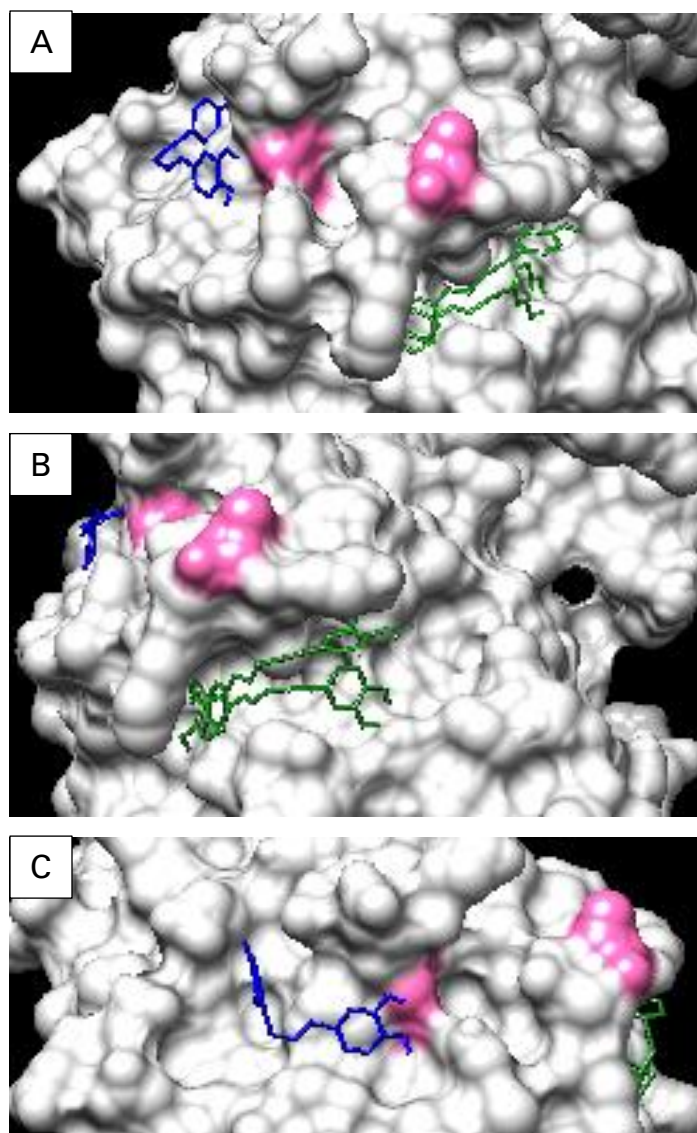


Figure 10: Alternative groove's box in p38 $\alpha$ . (1LEW crystal structure).



**Figure 11: Localization of the alternative groove and the DRS site in the 1LEW p38α crystal structure.** Cysteine residues are colored in pink. (A) rooperol in blue docked to the DRS and rooperol in green docked to the alternative groove. (B) rooperol in green docked to the alternative groove. (C) rooperol in blue docked to the DRS.

The same box was used in the different PDB files for different crystalline structures of p38α. Such structures were 1LEW<sup>34</sup>, 2Y80<sup>39</sup>, 2OZA<sup>38</sup>, 2ONL<sup>72</sup>, 2OKR<sup>72</sup>, 2LGC<sup>73</sup>, 1A9U<sup>74</sup>, 3TG1<sup>75</sup>, and 5UOJ<sup>19</sup>. Figure 12 shows the interactions between rooperol and the alternative groove in the crystal structure 1LEW of p38α.



**Figure 12: Docking between rooperol and the alternative groove in the crystal structure 1LEW of p38 $\alpha$ .**

The same docking procedure between rooperol and the different crystal structures of p38 $\alpha$  was done. The affinities obtained from the alternative groove in each structure and their comparison with the DRS site are showed in table 13.

**Table 13: Rooperol affinity with the alternative groove against affinity with the DRS.**

Crystal structure	DRS (kcal/mol)	Alternative groove (kcal/mol)
1LEW	-7.0	-6.1
1A9U	-7.2	-6.1
2LGC	-6.7	-6.2
2OKR	-6.5	-6.1
2ONL	-6.7	-6.3
2OZA	-6.5	-5.3
2Y8O	-6.9	-5.5
3TG1	-6.5	-5.2
5UOJ	-7.3	-6.1

In all the crystal structures the alternative groove obtained acceptable affinity energies. However, the values of the alternative groove were lower in energy than the values obtained for the DRS site in all the crystal structures. Therefore, the alternative groove was eliminated as an option for rooperol docking.

## **2. Horseradish Peroxidase Assay**

The initial work done in the HRP assay was to choose the right concentration of the HRP enzyme. The characteristics that the enzyme at the appropriate concentration should display are having an intense signal that last for a long period of time (30 to 60 min) with low variations. Another important point is that the signal should be readable in both instruments, in the chemidoc and in the plate reader. These two instruments were compared to measure the accuracy in both and, to choose the equipment that gives the most accurate measurements. Figures 13 and 14 show the intensity of luminescence obtained by the different concentrations of HRP at fixed concentrations of Luminol (5 mM) and peroxide (5.2 mM). The measured concentrations of HRP were 10, 5, 2.5, 1.25, 0.625, 0.3125, 0.156, 0.078, 0.039, 0.0195, all in mU. In addition, two negatives were measured, one with no enzyme, and the other with buffer only. The luminescence was measured by a plate reader and by a chemidock instrument for a period of time of 1 hour.

The luminescence displayed by the reaction of the HRP in contact with peroxide is shown until 0.3125 U of the HRP enzyme in both equipment. At lower quantity, the enzyme is too scarce to react with the peroxide. The main difference between both instruments is that the plate reader measures luminescence counts (intensity) while the chemidoc measures the sum of all the intensities within the band boundaries<sup>81</sup>. Therefore,

the luminescence measured by the plate reader tends to decrease over the time regardless of the concentration of the enzyme, while in the chemidoc there is not a clear tendency.

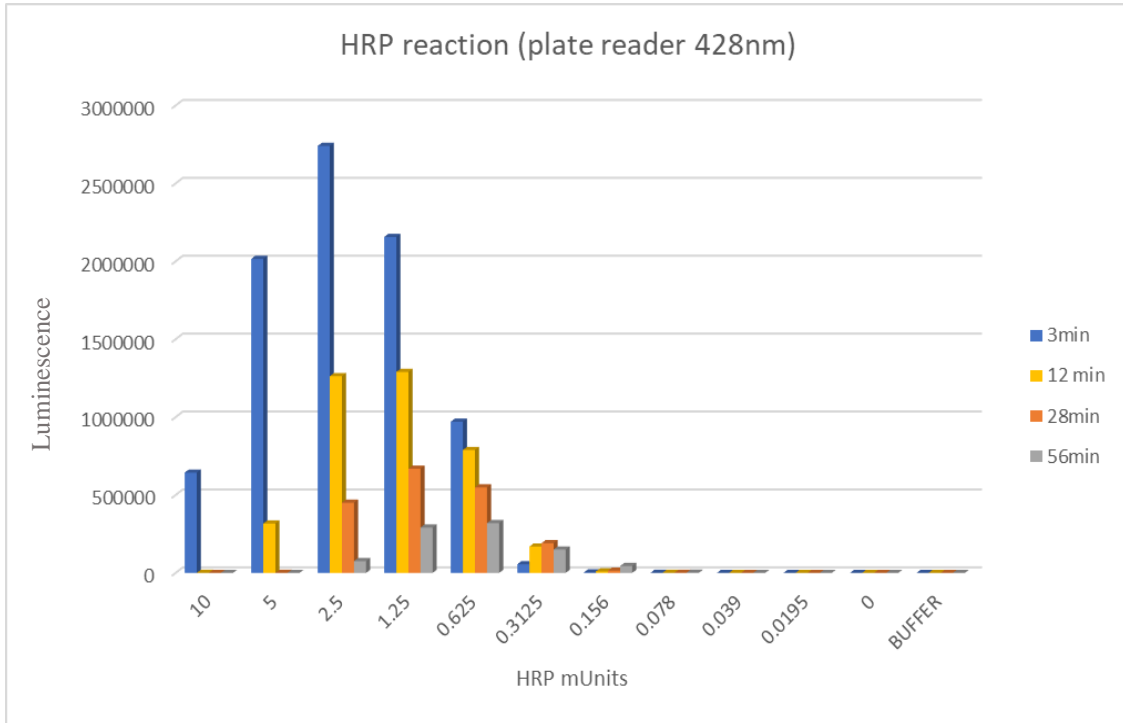


**Figure 13: Luminescence displayed by HRP at different concentrations for a period of one hour at room temperature.** Reading from the plate reader.

The signal from the point 0.625 mU was the smallest amount of enzyme measurable in both equipment for the entire time of one hour. Hence, this concentration was chosen for the next step. It is of great importance to notice that the plate reader has more sensitivity to smaller quantities of luminescence than the chemidoc. It measured intensity from the wells containing only 0.3125 and 0.125 mU of the enzyme, while the chemidoc was not able to measure such small quantities of enzyme.

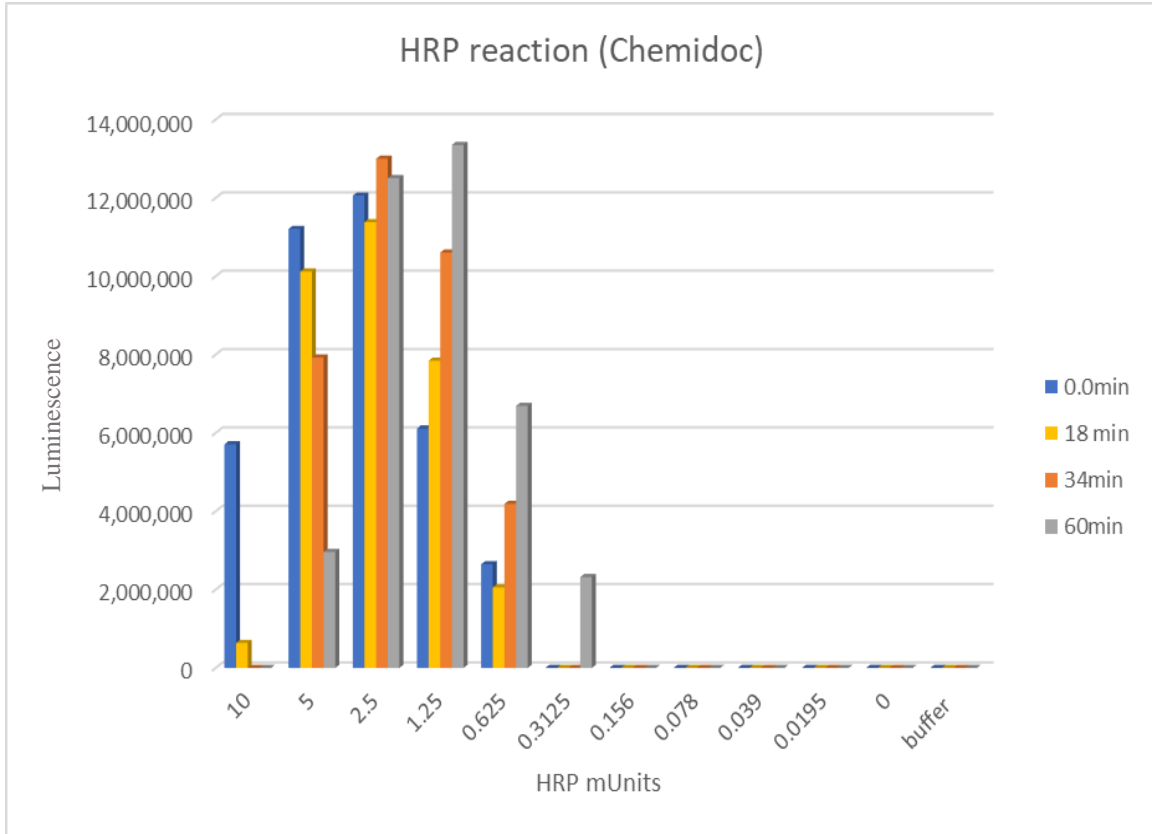


**Figure 14: Luminescence displayed by HRP at different concentrations for a period of one hour at room temperature. Reading from the chemidoc.**

In the second part of the HRP assay the accuracy from chemidoc against plate reader was compared at a fixed concentration of HRP (0.625 mU). The results obtained from such experiment are shown in figure 15 and 16. In the plate reader, the signal show a tendency to decrease over the time. Also, this equipment shows that the standard deviation also decreases over the time. In comparison, the signals shown by the chemidoc shows almost the same intensity all the time. This is because of the difference in reading methods of the equipment. The plate reader makes a direct reading of the luminescence while the chemidoc uses an imaging system in which a scale of shades is used to define the brightest sample and the darkest sample. The rest of the samples are measured to fit in such scale. In addition, the chemidoc measures the sum of all the intensities within the

band boundaries. Therefore, the measurements made with the chemidoc were constant almost all the time. It is important to mention that the standard deviations from the plate reader decrease over the time while the Chemidoc shows larger standard deviations that do not decrease over the time. Therefore, the plate reader shows more accurate results than the chemidoc.

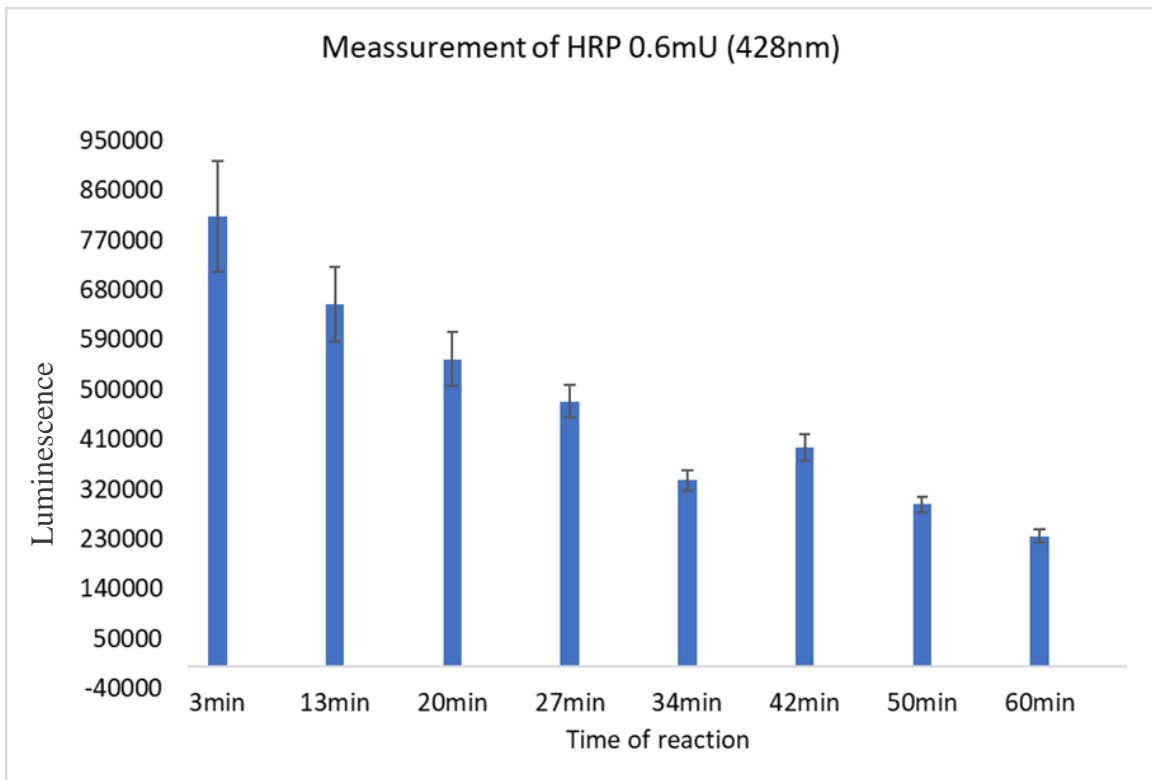


**Figure 15: Luminescence displayed by HRP (0.625 mU) for a period of one hour at room temperature. Reading from the plate reader.**

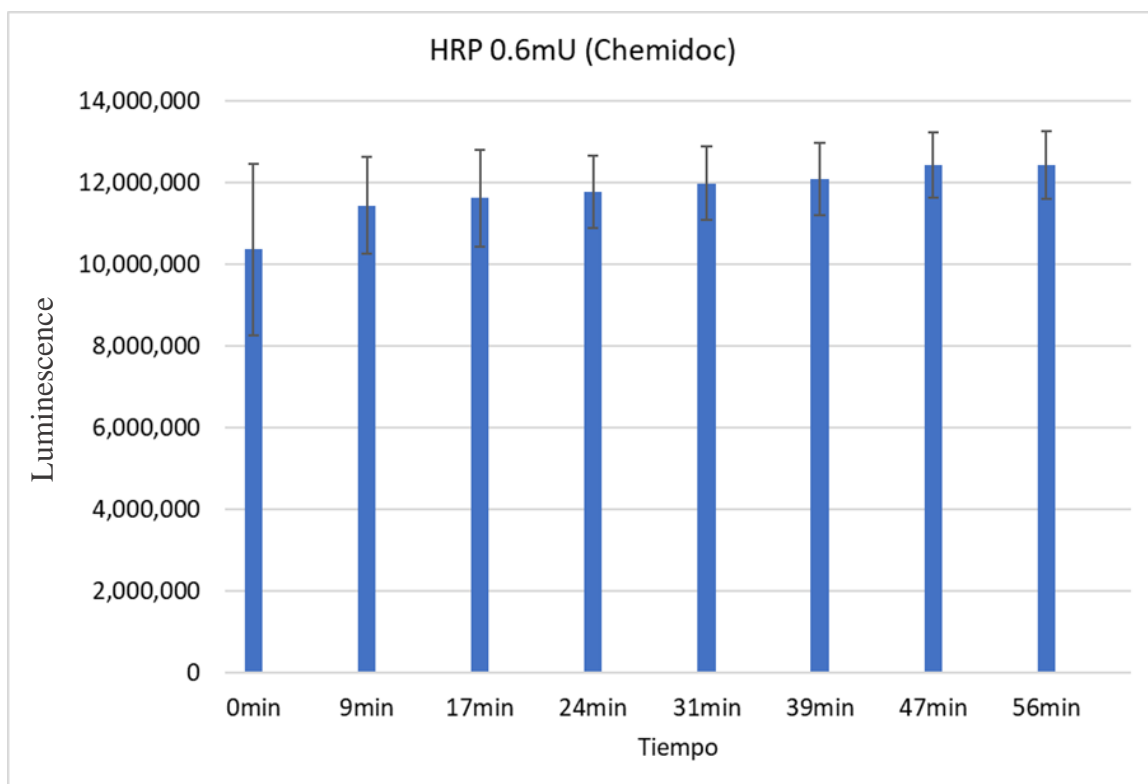


**Figure 16: Luminescence displayed by HRP (0.625 mU) for a period of one hour at room temperature. Reading from the chemidoc.**

The signal to noise (S/N) of the two instruments was measured as a third part of the HRP assay. Therefore, 20 repetitions of the HRP solution (0.625 mU) and 20 repetitions of buffer were measured at different times for a period of one hour. The results obtained are shown in figures 17 and 18. In the case of the plate reader the largest S/N was obtained at the first reading, but it had also the largest standard deviation. However, as the time progressed the standard deviation decreased significantly and the S/N along with it. Nevertheless, the lowest S/N was 177, which is an acceptable value.

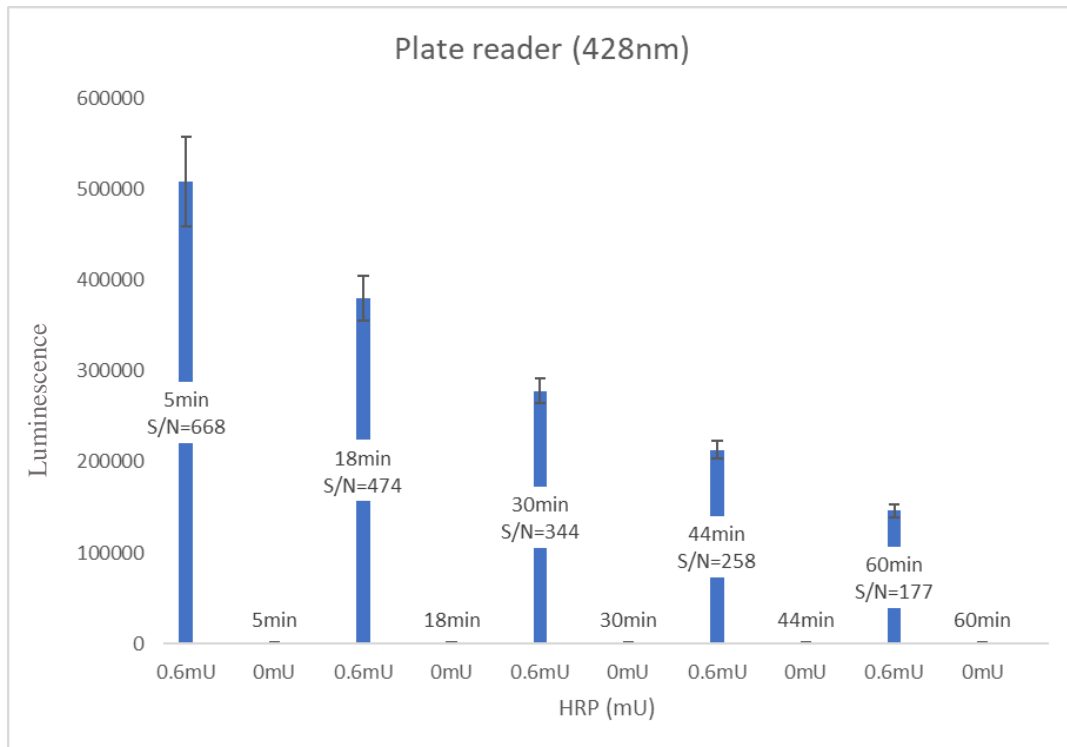


**Figure 17: Luminescence displayed by HRP (0.625mU) against buffer for a period of one hour at room temperature. Reading from the plate reader.**

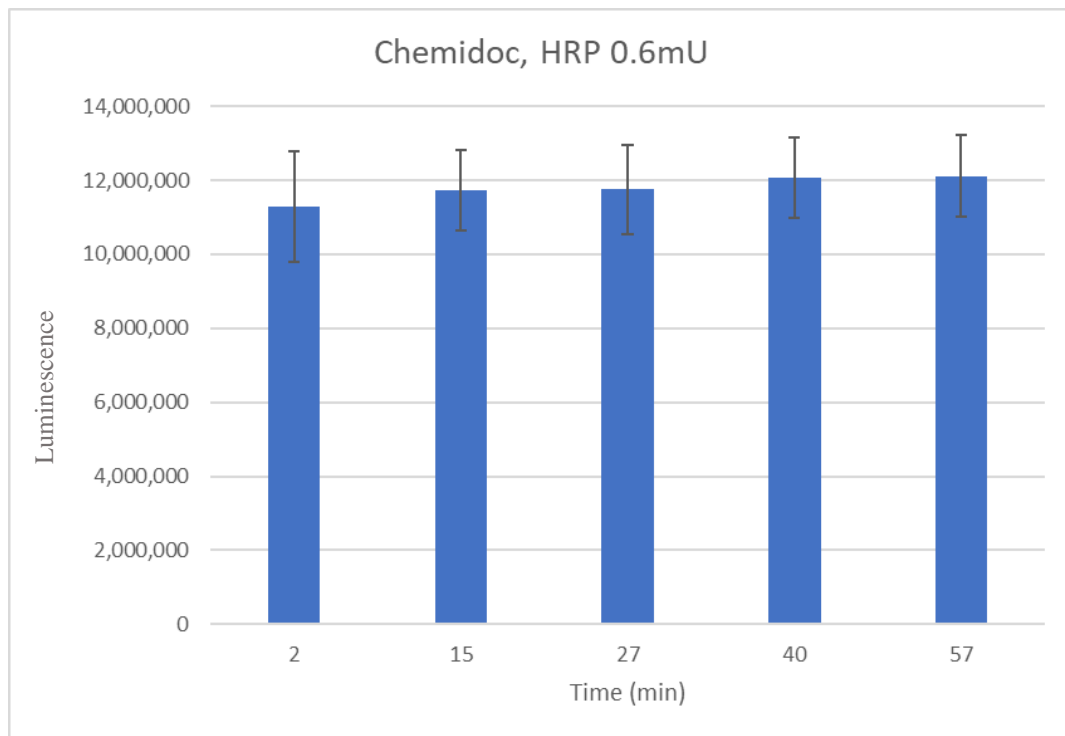


**Figure 18: Luminescence displayed by HRP (0.625 mU) against buffer for a period of one hour at room temperature. Reading from the chemidoc.**

In the case of the chemidoc, the wells filled with buffer could not be read by the instrument. This was because the method that the chemidoc uses is not suitable to read samples with no luminescence. As mentioned before, the chemidoc uses an imaging system that measure the samples in a scale of shadows. The equipment defines the brightest sample and the darkest sample, and then, it fits the rest of the samples in such scale. In this case the buffer was out of the scale. Thus, the values for the background were not measured and the S/N was not calculated. However, the chemidoc exhibited very constant signals with constant standard deviations but such values were larger than those displayed by the plate reader. Thus, for the next steps the plate reader was used as the main equipment to detect luminescence.

In the fourth part of the HRP assay the different modes of dispensing performed by the pipetting robot were compared to select those that displayed the lowest error. The parameters compared were pre-wet tip, touch tip, tip position, multi-dispense, and mixed volume. The detailed procedure for this step was described in the experimental section of this work. The results obtained by the plate reader are shown in figure 19 and 20.

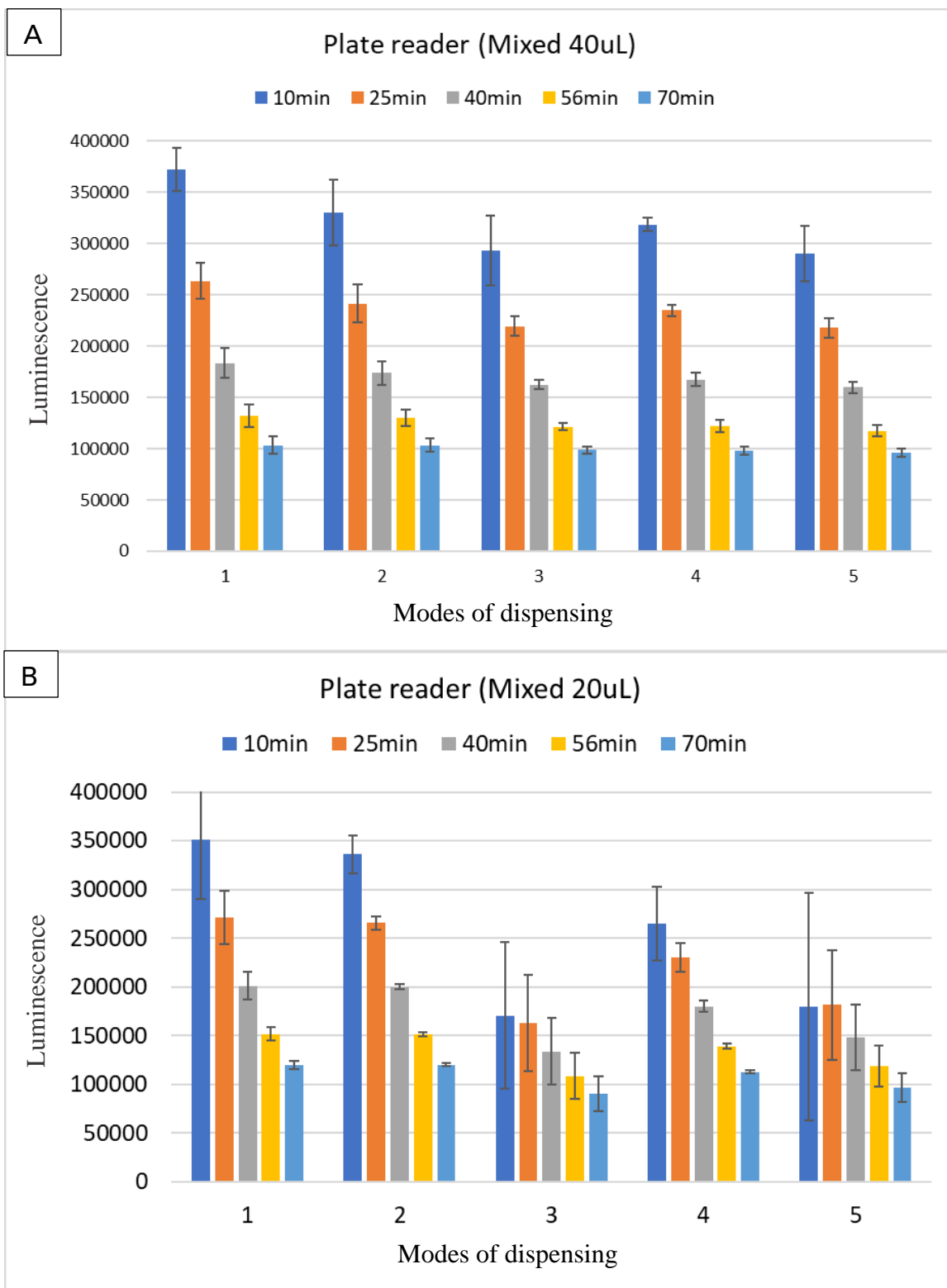


**Figure 19: Comparison of the five different modes of dispensing HRP solution. A)** reaction mixed using 40 $\mu$ L of mixing volume. **B)** reaction mixed using 20 $\mu$ L of mixing volume. Reading made by the plate reader at room temperature.

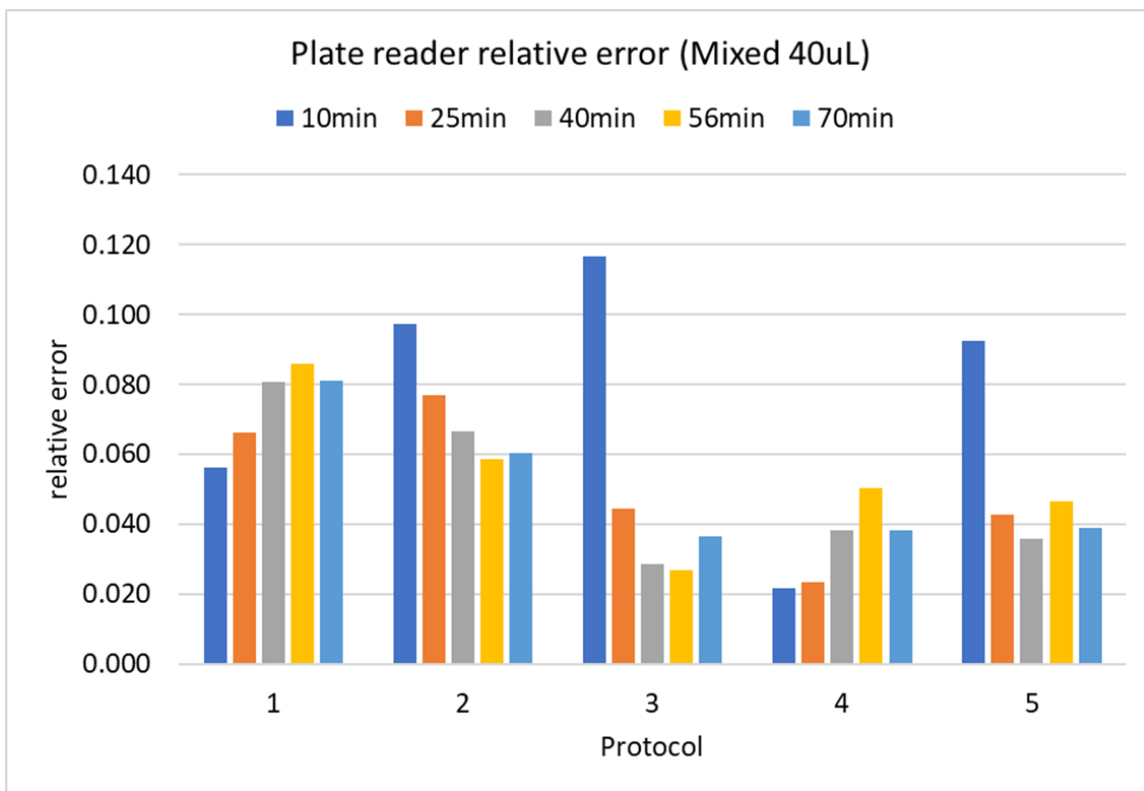


**Figure 20: Comparison of the relative error of the five different modes of dispensing HRP solution when using 40 $\mu$ L of mixing volume.** Reading made by chemidoc for a period of 70 mins at room temperature.

In general, the wells mixed with 20  $\mu$ L (half of the total reaction volume) as a mixing volume showed greater standard deviations in both equipment than when mixing 40  $\mu$ L (total reaction volume). Therefore, it is always better to mix the complete volume of the reaction. To compare the different modes of pipetting HRP when mixing the total reaction volume, the relative error was calculated for each one of the dispensing modes (figure 20). In mode 1 (no pre-wet tip): relative error is larger than modes 3, 4, and 5, and increased over time. Thus, this mode was discarded. For the mode 2, the relative error was larger than modes 3, 4, and 5, but it decreased over the time. This is a desirable behavior. The mode 3 (multi dispense) in this experiment showed promising results for the relative error, but when it was used for other experiments it gave undesirable results.

The multi dispense mode always gave higher signal in the first well of the multi dispensed wells. Thus, this mode was eliminated as an option when using the pipetting robot. When using the mode 4 (1 mm tip position from the bottom of the well) in this experiment the relative error was low, but when this mode was used for smaller volumes, it produced some problems. When the volumes were very small (as the volumes used for the ADP-Glow: 1, 2, 3, and 5  $\mu\text{L}$ ) the robot's pipette was not able to aspirate, mix, and transfer solutions. Thus, it is always better to lower the pipette to the minimum distance from the bottom of the well which is 0.5 mm. The mode 5 (no touch tip) also gave undesirable results in other experiments as it produced large standard deviations. Therefore, the mode 2 (pre-wet tip, touch tip, tip position 0.5 mm, no multi-dispense, and mix total volume) was the chosen one because it gave the smaller standard deviations and more stable signals.

### **3. Standardization of The ADP-Glow Reaction**

In the firsts attempts to reproduce the results showed in the article of Zegzouti H, using the ADP-Glow reaction, the results were not satisfying. In general, this was because the linearity and the S/N was poor each time the reaction was run. Figures 21 and 22 are examples of the curves obtained following the steps from Zegzouti H.

The first 5 points of the ATP-ADP conversion curve (1, 2, 4, and 5%) show not linear behavior while the points at 40, 80, and 100% conversion showed large standard deviation. In addition, the signal to noise ratio is very low with a value of 2.8 due to very high signal of 0% point. On the other hand, the hexokinase conversion curve shows similar behavior to the results obtained by Zegzouti H. However, the main problem was

that there was not much difference in signal between the 10 mU and the 0.001 mU due to the low S/N ratio. In other words, in this experiment, the assay had low sensitivity.

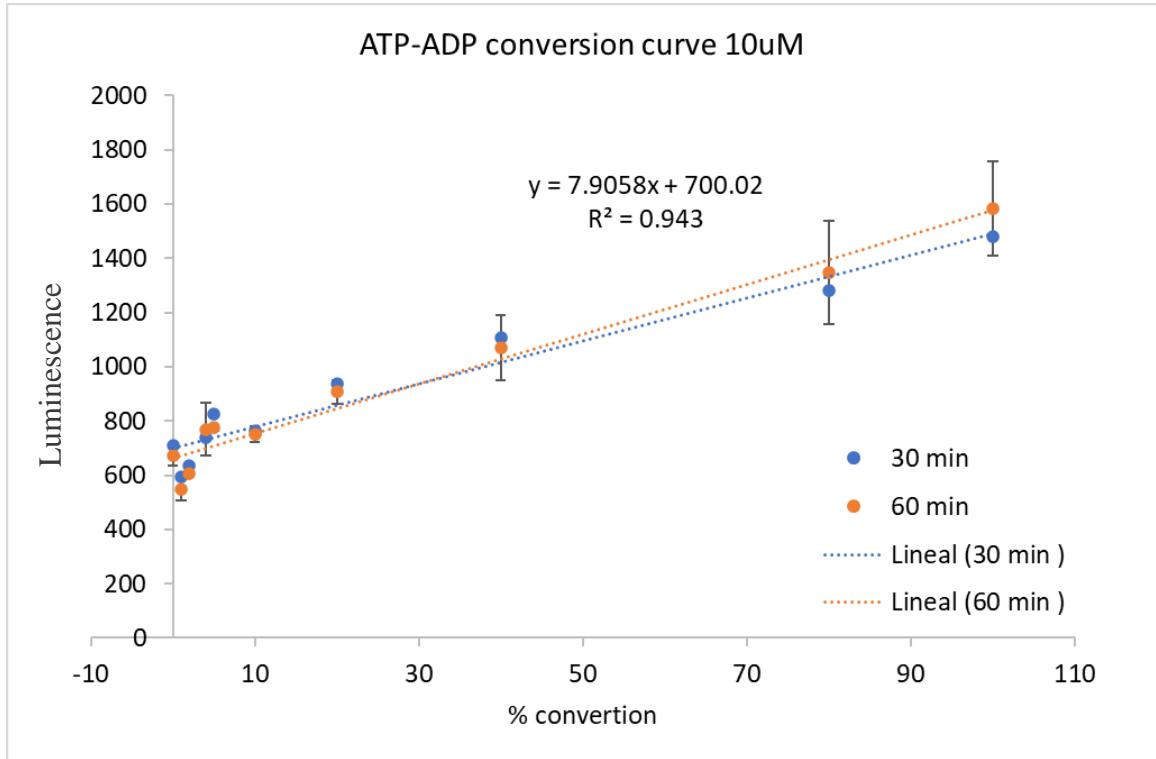


**Figure 21: Example of the ATP-ADP conversion curve obtained during the first attempt to reproduce Zegzouti H results.** Experiment made at 10  $\mu$ M concentration of ATP/ADP and measured at 30 and 60 mins at room temperature.  $Z'$  value at 30 min was 0.1, and at 60 min was 0.3. Such results meant that the separation band is small, this is not an ideal assay.

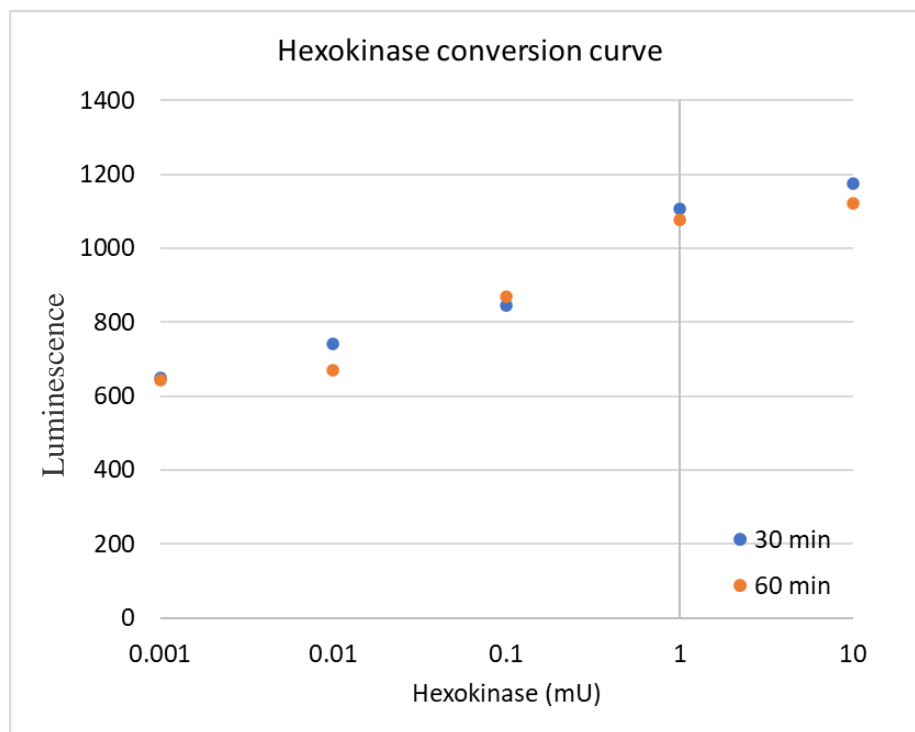


**Figure 22: Example of the HK curve obtained during the first attempt to reproduce Zegzouti H results.** Experiment made at 10  $\mu$ M concentration of ATP/ADP and measured at 30 and 60 mins at room temperature.  $Z'$  value at 30 min was 0.007, and at 60 min was -0.293. Such results meant that there is not separation band and that the screening is impossible with this assay.

For the second attempt to reproduce the results from Zegzouti H, the protocol for the robot was optimized. The procedure to obtain the ATP-ADP percent conversion curve was modified. Instead of pipetting different volumes of the ATP and ADP to each well, a series of dilutions 1:1 was made. The points of ADP percent conversion curve were: 100, 50, 25, 12.5, 6.25, 3.125, 1.562, and 0.781. Figures 23 and 24 shows the results obtained on the second attempt to reproduce the data from Zegzouti H.

The corrected ATP-ADP percent conversion curve showed an acceptable linearity, around 0.99 for each ran plate. Also, the S/N greatly improved with values around 50. The values obtained for S/B were around 20, and for Z were 0.9. All this data signified that the modified procedure to obtain an ATP-ADP curve using the pipetting

robot was excellent. Therefore, we proceed to adapt the procedure to the desired conditions for reactions with p38 $\alpha$ . The enzyme curve also showed improvement by having more defined points and less noise.

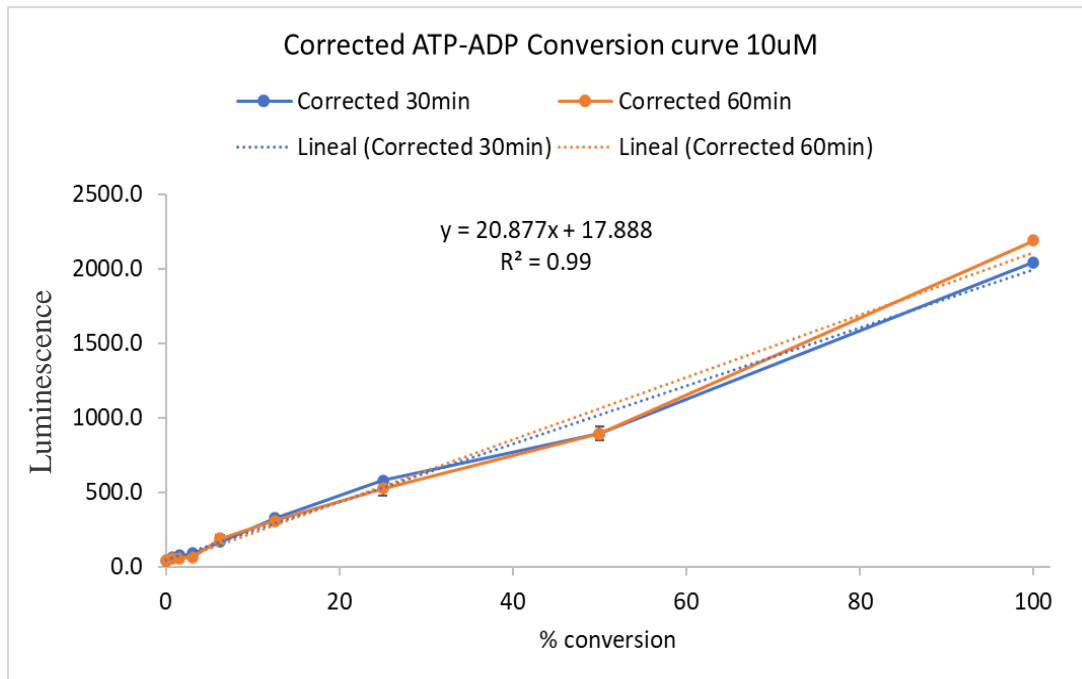


**Figure 23: ATP-ADP conversion curve obtained during the second attempt to reproduce Zegzouti H results.** Experiment made at 10  $\mu$ M concentration of ATP/ADP and measured at 30 and 60 mins at room temperature. Z' value at 30 and 60 min was 0.9. Such result meant that the separation of the bands is large, and it is an excellent outcome.

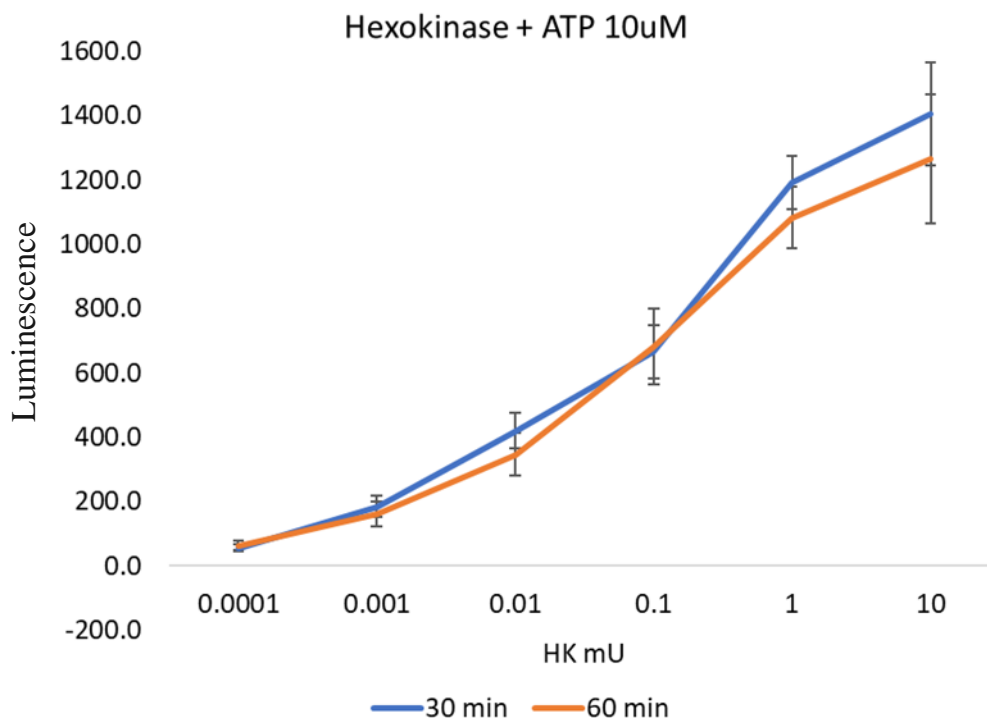


**Figure 24: HK conversion curve obtained during the second attempt to reproduce Zegzouti H results.** Experiment made at 10  $\mu$ M concentration of ATP and measured at 30 and 60 mins at room temperature. Z' value was 0.5. Such result meant that the separation of the bands is large, and it is an excellent outcome.

For the second step, the influence of the solvent, DMSO, in the reaction was measured. Thus, a concentration of HK was selected in based of the HK curves obtained from the previous step. Such concentration was 0.1 mU of HK, that corresponds to the inflection point of the HK curve. The different concentrations of DMSO investigated were 10, 5, 2.5, 1.25, 0.625, and 0 percent. Figures 25 and 26 show the results obtained. During this experiment any of the different concentrations of the DMSO have a significant difference. Therefore, the contribution of the DMSO to the ADP-Glow reaction is negligible.

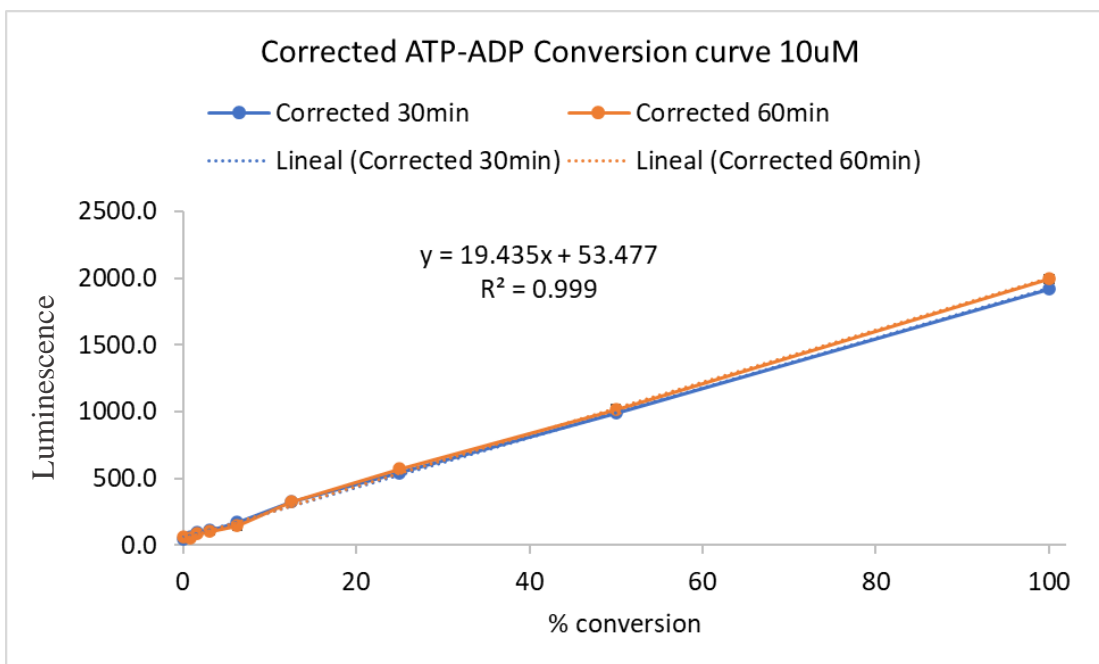


**Figure 25: ATP-ADP conversion curve obtained during the second step (measuring DMSO effect).** Experiment made at 10  $\mu$ M concentration of ATP and measured at 30 and 60 mins at room temperature. Z' value was 0.9. Such result meant that the separation of the bands is large, and it is an excellent outcome.

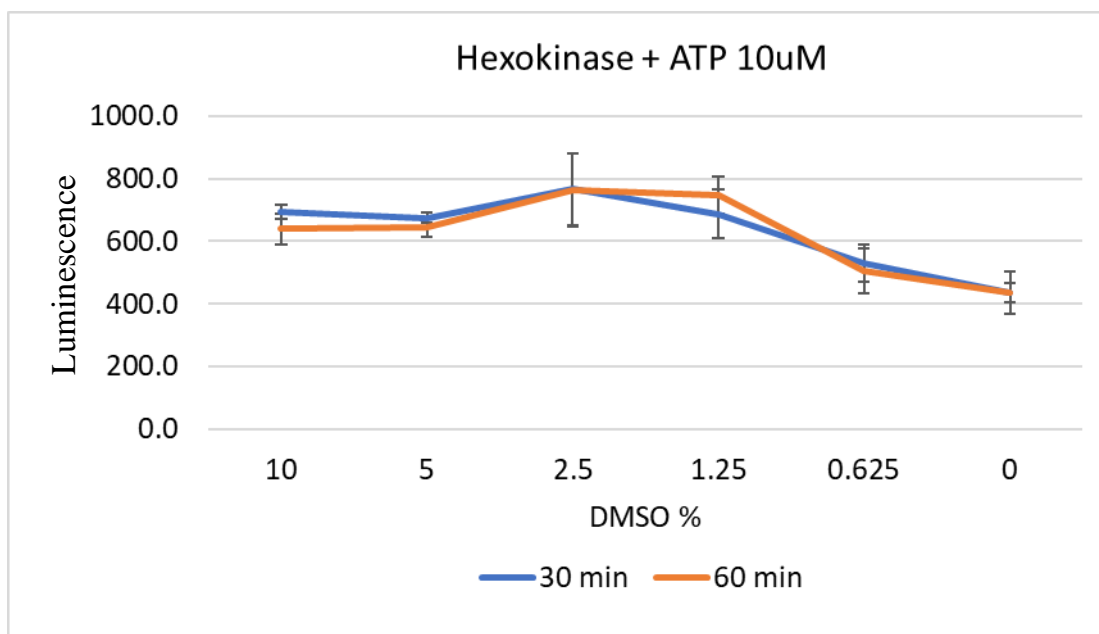


**Figure 26: DMSO effect in the ADP-Glow reaction.** Conditions of the reaction: HK 0.1 mU and ATP 10  $\mu$ M. Experiment made at 10  $\mu$ M concentration of ATP and measured at 30 and 60 mins at room temperature. Z' value was -1, -2. Such result meant that the bands overlap, and it is impossible to screen.

In the third step a correction of the ATP-ADP conversion curve was made. In previous steps the ATP concentration was kept constant instead of decreasing when the ADP increased. For that reason, it was necessary to make a correction to produce a standard curve with the adequate concentrations of ATP and ADP. In figure 27 the results obtained by the corrected ATP-ADP percent conversion curve are displayed. In this figure is possible to observe how the ATP decreased as the ATP increased. This variation of the ATP was achievable by doing a series of dilutions of ATP described previously in the experimental part in table 8 and 9.

The corrected percent conversion curve showed acceptable results in all the parameters measured. The value of the  $R^2$  was 0.981, S/N was 430, S/B was 141, and Z factor was 0.9. All these values indicate that the corrected conversion curve obtained using the robot is an excellent assay. Therefore, the next step was to test p38 $\alpha$ .

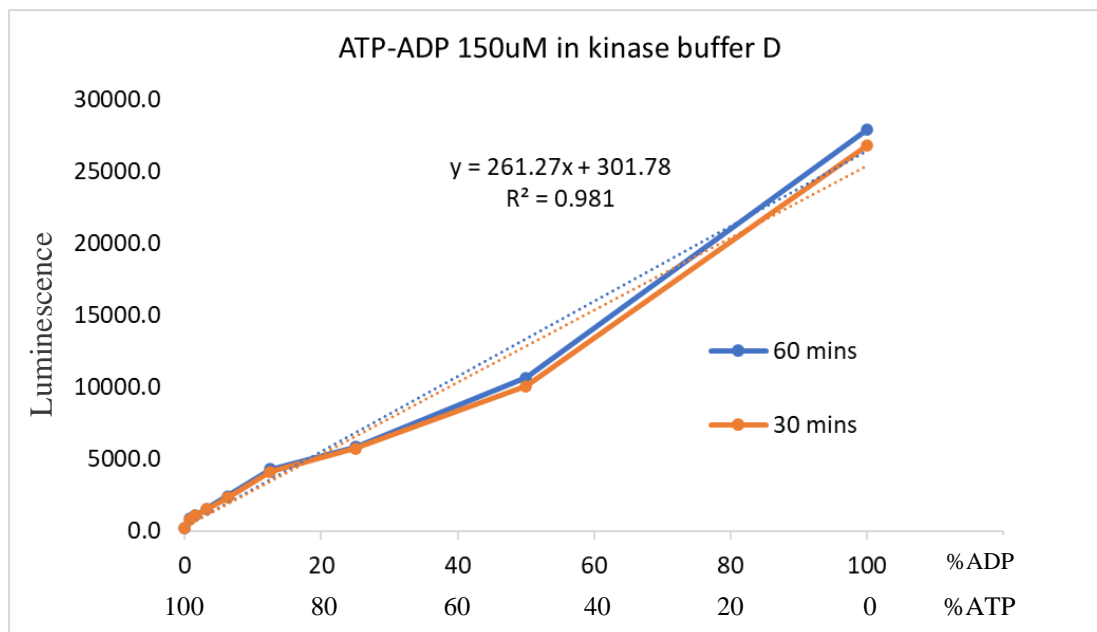


**Figure 27: Second correction of the ATP-ADP percent conversion curve.** Conditions of the reaction: ATP/ADP 150  $\mu$ M, 1% DMSO, measurements at 30 and 60 mins, reaction conducted at room temperature. Z' value equal to 0.9.

The fourth step was to test p38 $\alpha$  activity with MBP as a substrate. Thus, 10 points of different concentrations of p38 $\alpha$  were done as part of the experiment. The measured concentrations were: 30, 15, 7.5, 3.35, 1.875, 0.9375, 0.4687, 0.2343, 0.117, and 0 ng of the enzyme. The concentration of the Substrate solution was constant for the entire experiment (0.1 mg/ $\mu$ L of MBP). Figure 28 shows the results of this experiment. Surprisingly, the enzyme showed very low activity and very high standard deviation in the low concentrations of the enzyme. There could be several reasons for having low enzyme activity. Enzymes are usually very delicate and vigorous movements, such as mixing with vortex mixer, could cause denaturalization of the enzyme. Other reasons could be the time of the reaction. If the enzyme is waiting for a long period of time to be used it is possible that inactivation occurs. Another reason is temperature, p38 $\alpha$  has shown high activity in temperatures around 30-37°C<sup>80</sup>. In this case, the high variation in the low concentrations of the enzyme could be due to a spinning problem. The volumes used for the p38 $\alpha$  solution were so small that, to ensure having all the available volume in just one place, the Eppendorf tube was centrifuged. This could produce the agglomeration of the enzyme in the tip of the tubes causing an inhomogeneous solution. Also, once the dilutions of the enzyme were done in the plate, the plate was also shaken and then centrifuged. This possibly produced agglomeration of the enzyme in the bottom of the wells, too. This problem was more visible at lower concentrations because one well obtained most of the enzyme while the others got almost nothing. Thus, the variation was large for the smaller concentrations of the enzyme. The only two reliable points were the most concentrated: 15 ng and 30 ng. Therefore, the concentration of 30 ng was chosen to work with p38 $\alpha$ .

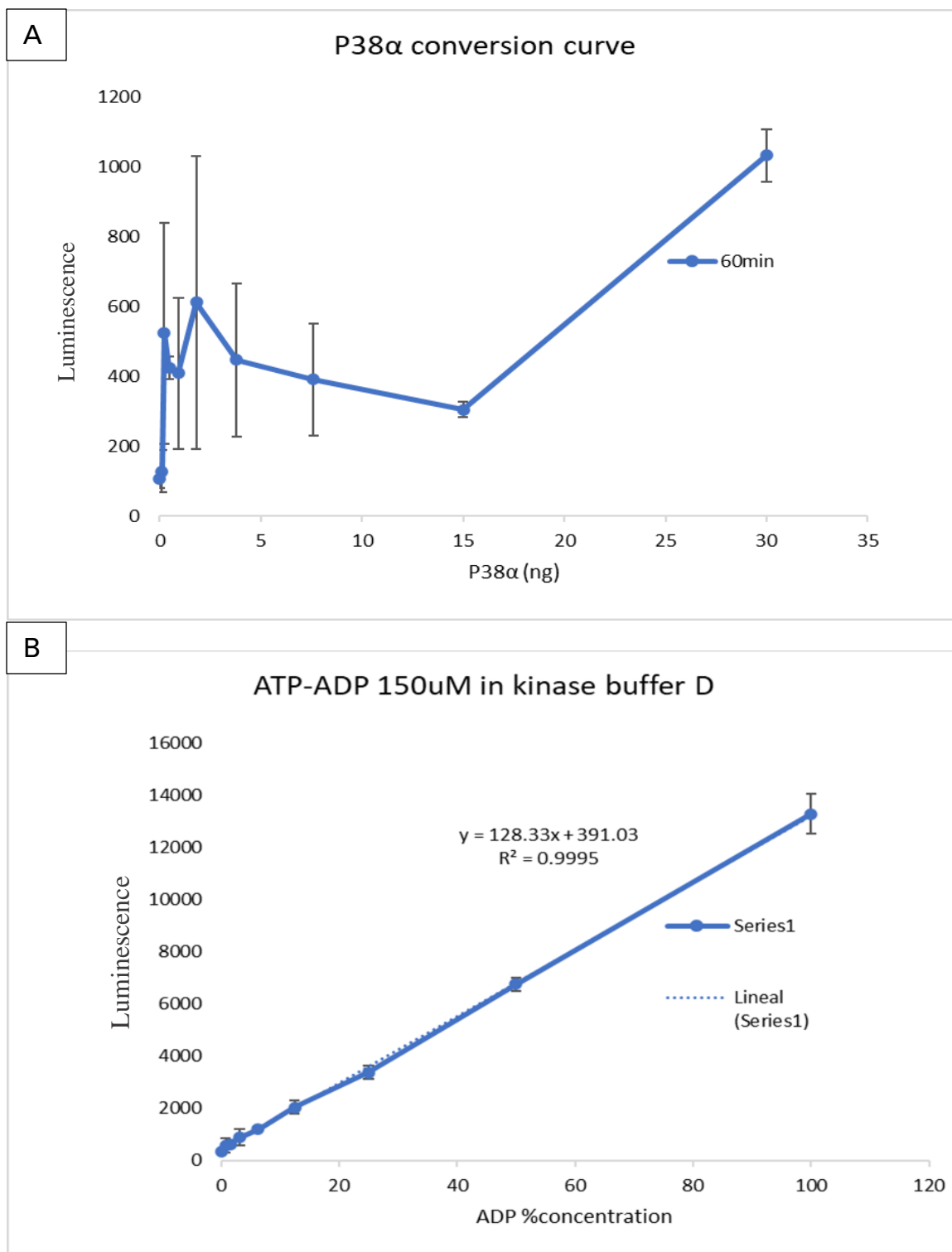


**Figure 28: p38 $\alpha$  conversion curve at a constant concentration of MBP.** A) p38 $\alpha$  results. B) ATP-ADP percent conversion curve for this experiment. Conditions of the reaction: ATP/ADP 150  $\mu$ M, 1% DMSO, measurement at 60 mins, reaction conducted at room temperature. Z' value for the ATP-ADP conversion curve equal to 0.9. Z' value for the p38 $\alpha$  conversion curve equal to 0.55.

In the fifth step, different concentrations of the substrate MBP were tested to observe which concentration produced more activity with p38 $\alpha$ . The concentrations of MBP managed in this experiment were 0.5, 0.4, 0.3, 0.2, and 0.1mg/mL. The results obtained in this step are shown in figure 29.

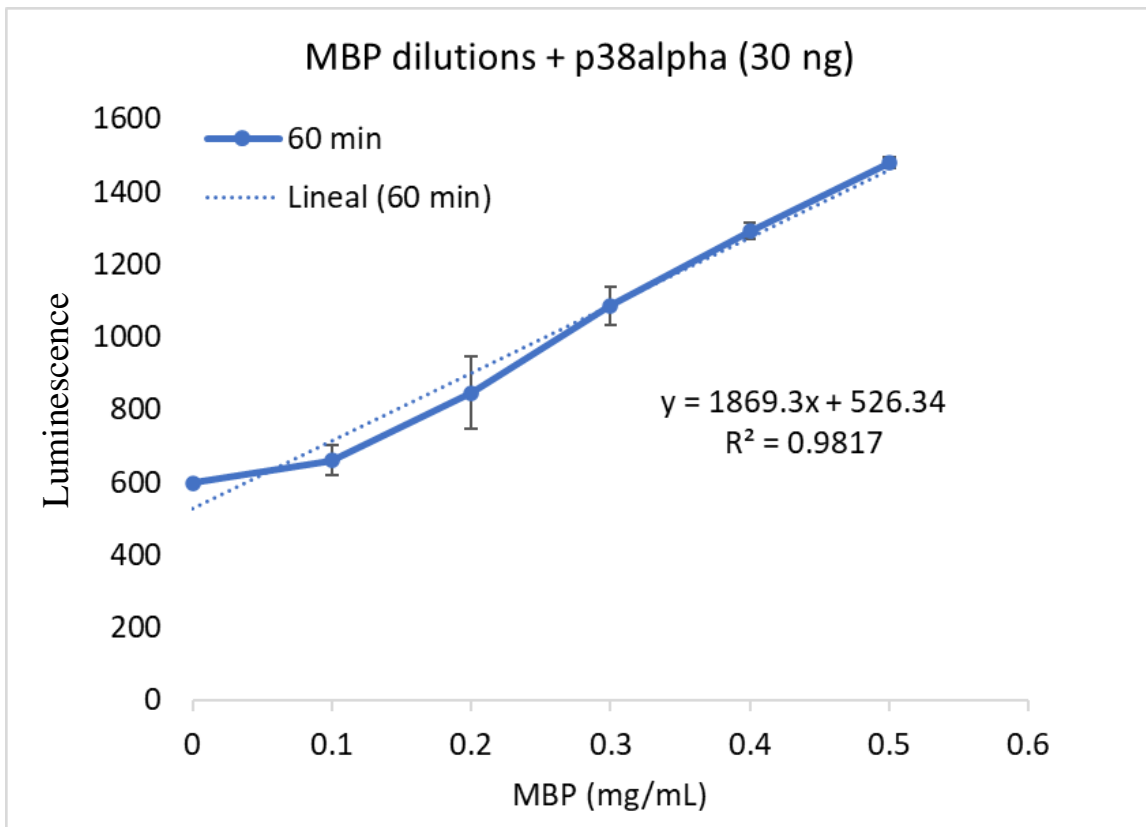


**Figure 29: p38 $\alpha$  conversion curve with different concentration of MBP.** Conditions of the reaction: ATP 150  $\mu$ M, 1% DMSO, 30 ng of p38 $\alpha$ , measurement at 60 mins, reaction conducted at room temperature. Z' value for the p38 $\alpha$  conversion curve equal to 0.9.

The enzyme showed increased luminescence as concentration of MBP increased. The higher signal was obtained with 0.5mg/mL of MBP that corresponds to 5.71% ADP conversion. These results showed that the enzyme was more active at higher concentrations of MBP. Unfortunately, this was the highest concentration manageable in this experiment. Therefore, 0.5mg/mL was the concentration selected to work with the

enzyme.

In the sixth step different concentrations of the inhibitor staurosporine were tested against p38 $\alpha$ . The concentrations tested were 500000, 100000, 20000, 4000, 800, 160, 32, 6.4, 1.28, and 0.256 nM of staurosporine. The concentration of the p38 $\alpha$  was constant at 20 ng. Figure 30 shows the results obtained from this experiment. Unfortunately, in this experiment the inhibitor did not show activity because all the dilutions were in the same range of the 0.0 nM of inhibitor. These results could be due to the small volumes managed in this reaction. The volume pipetted for the inhibitor is just one  $\mu$ L. During the validation of the pipetting robot system such small volumes were not tested. Therefore, there is no certainty that the robot is dispensing one  $\mu$ L of the inhibitor. It is possible that such small volume got attached to the pipette just to be discarded along with the tip into the trash. Another reason for the low activity from the inhibitor is that the reagent was already spoiled or was spoiled during the procedure to obtain the stock solution (the reagent was mixed with DMSO to obtain a solution). However, there was a significant difference between the blank (0.0 nM of inhibitor) and the negative (without enzyme). This meant that the enzyme was working. More work with the inhibitor is necessary to find the crucial conditions to observe activity from the inhibitor.

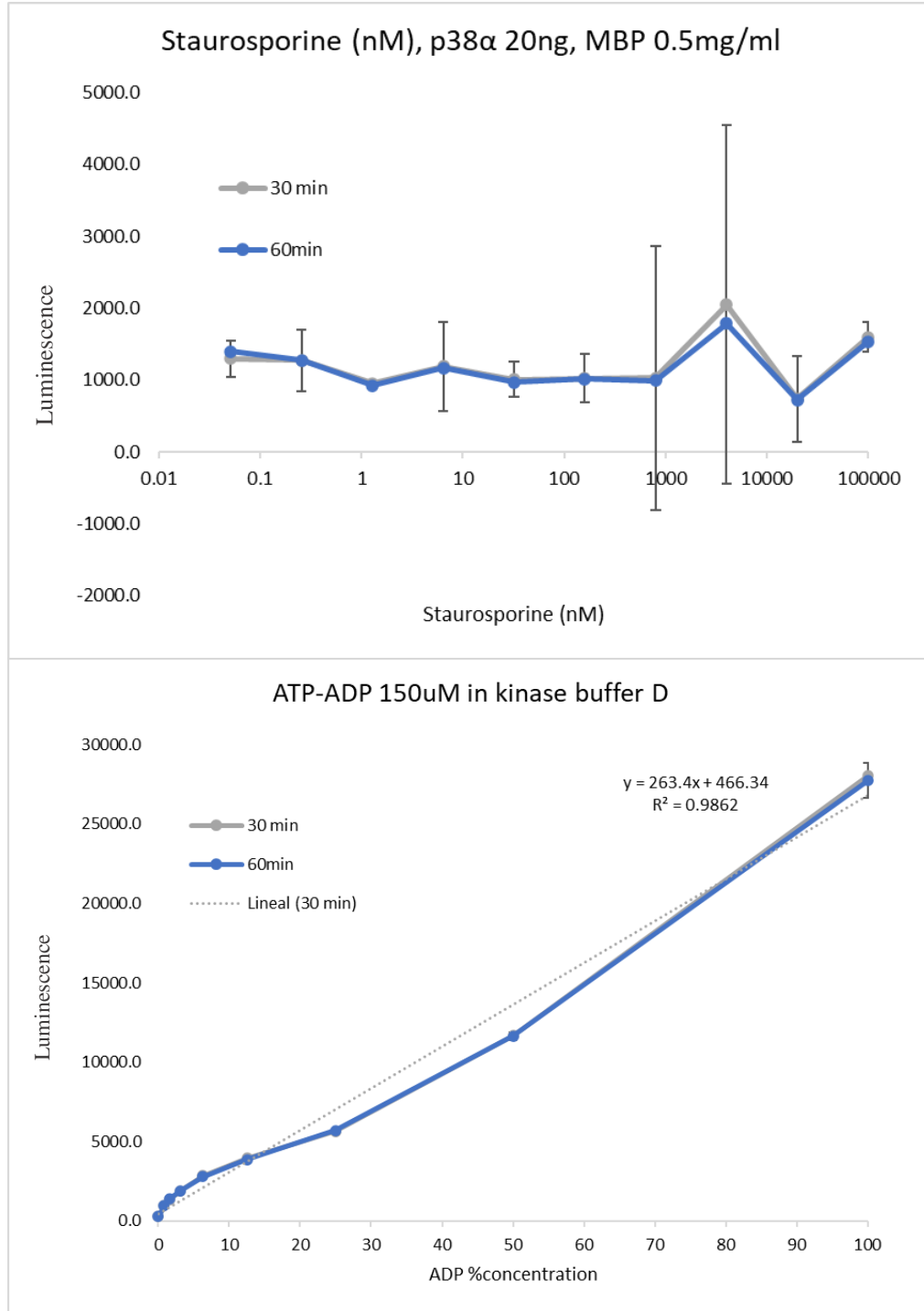


**Figure 30: p38α conversion curve with different concentration of staurosporine.** A) p38α with staurosporine results. B) ATP-ADP percent conversion curve for this experiment. Conditions of the reaction: ATP 150 μM, 1% DMSO, 20 ng of p38α, 0.5 mg/ml MBP, measurement at 30 and 60 mins, reaction conducted at room temperature. Z' value for the p38α conversion curve equal to -0.6.

## IV. CONCLUSIONS

For the first part of this project a docking of p38 $\alpha$  with rooperol was conducted. A groove close to the DRS site called the alternative groove was analyzed. Surprisingly, in all the crystal structures the alternative groove obtained acceptable but lower values than those obtained for the DRS. Therefore, the alternative groove was eliminated as an option for rooperol docking and should not be explored in the future.

For the HRP assay, it can be concluded that the plate reader and the chemidoc exhibited comparable results. Nevertheless, the plate reader was more sensitivity to low quantities of luminescence than the chemidoc. Another large difference is the method in which each instrument measures luminescence. The plate reader measures total intensity while the chemidoc measures the sum of all the intensities within the band boundaries. For the second part of the HRP assay, it can be concluded that the plate reader shows more accurate results. In addition, in the third part of the HRP assay, it was found that the plate reader displays larger S/N than the chemidoc. In the fourth part of this assay, it was concluded that the appropriate characteristics of pipetting, when using the robot, to obtain low standard deviation were: pre-wet tip or, touch tip, tip position 0.5mm, no multi-dispense, and mix total volume.

To standardize the ADP-Glow reaction using the pipetting robot, it was necessary to reproduce the results obtained by Zegzouti H. These results showed the normal behavior of the ADP glow reaction when it is used to measure different kinases. In this experiment the hexokinase was taken as a basis to adapt the ADP-glow assay to the pipetting robot. In the first attempt to reproduce the results from the article of Zegzouti H,

it was discovered that to obtain similar results as the results obtained in that study, it was necessary to change the procedure of the ATP-ADP conversion curve. During the second step to standardize and to adapt the ADP-Glow reaction to the use of the pipetting robot, the effect of the DMSO solvent was measured. The result of this experiment showed that the contribution of such solvent is negligible. The third step was to make a new correction in the ATP-ADP percent conversion curve. In previous steps the concentration of the ATP was kept constant when doing the ATP-ADP percent conversion curve. Thus, a corrected curve in which the concentrations of the ATP and ADP were correct for all the curve points was built. In this final arrangement of the conversion curve the obtained parameters values were  $R^2=0.981$ ,  $S/N=430$ ,  $S/B=141$ , and  $Z=0.9$ . Such values meant that the protocol for the assay was excellent and ready to test p38 $\alpha$ . Thus, the protocol to obtain the conversion curve was always the same for the rest of the steps. In step number fourth, it was found that the enzyme does not have high activity in presence of MBP. Therefore, the amount of p38 $\alpha$  selected to keep working was 30 ng; the highest concentration tested. In the fifth step various concentrations of the MBP substrate solution were tested to find an optimal concentration of this solution. The concentration that showed the highest signal was 0.5mg/mL of MBP. Therefore, such concentration was selected to work with the enzyme. In the sixth step several concentrations of the inhibitor staurosporine were tested against p38 $\alpha$ . In this experiment the results showed no inhibitor activity. Therefore, it is necessary to perform more experiments with the inhibitor to find the appropriate conditions to observe inhibition of p38 $\alpha$ .

## LITERATURE CITED

1. Manning, G., Whyte, D. B., Martinez, R., Hunter, T. & Sudarsanam, S. The protein kinase complement of the human genome. *Science* vol. 298 1912–1934 (2002).
2. Hunter, T. Protein Kinase Classification. *Methods Enzymol.* **200**, 3–37 (1991).
3. Goldsmith, E. J., Akella, R., Min, X., Zhou, T. & Humphreys, J. M. Substrate and docking interactions in serine/threonine protein kinases. *Chemical Reviews* vol. 107 5065–5081 (2007).
4. Hanks, S. K. & Quinn, A. M. Protein Kinase Catalytic Domain Sequence Database: Identification of Conserved Features of Primary Structure and Classification of Family Members. *Methods Enzymol.* **200**, 38–62 (1991).
5. Peti, W. & Page, R. Molecular basis of MAP kinase regulation. *Protein Science* vol. 22 1698–1710 (2013).
6. Yueh, C. *et al.* Kinase atlas: Druggability analysis of potential allosteric sites in kinases. *J. Med. Chem.* **62**, 6512–6524 (2019).
7. Kim, E. K. & Choi, E. J. Pathological roles of MAPK signaling pathways in human diseases. *Biochimica et Biophysica Acta - Molecular Basis of Disease* vol. 1802 396–405 (2010).
8. Coulthard, L. R., White, D. E., Jones, D. L., McDermott, M. F. & Burchill, S. A. p38MAPK: stress responses from molecular mechanisms to therapeutics. *Trends in Molecular Medicine* vol. 15 369–379 (2009).

9. Jiang, Y. *et al.* Characterization of the structure and function of the fourth member of p38 group mitogen-activated protein kinases, p38 $\delta$ . *J. Biol. Chem.* **272**, 30122–30128 (1997).
10. Raman, M., Chen, W. & Cobb, M. H. Differential regulation and properties of MAPKs. *Oncogene* vol. 26 3100–3112 (2007).
11. Eid, S., Turk, S., Volkamer, A., Rippmann, F. & Fulle, S. Kinmap: A web-based tool for interactive navigation through human kinome data. *BMC Bioinformatics* **18**, 16 (2017).
12. Bajusz, D., Ferenczy, G. G. & Keseru, G. M. Structure-based Virtual Screening Approaches in Kinase-directed Drug Discovery. *Curr. Top. Med. Chem.* **17**, (2017).
13. Gross, S., Rahal, R., Stransky, N., Lengauer, C. & Hoeflich, K. P. Targeting cancer with kinase inhibitors. *J. Clin. Invest.* **125**, 1780–1789 (2015).
14. González-Medina, M. *et al.* Promiscuity analysis of a kinase panel screen with designated p38 alpha inhibitors. *Eur. J. Med. Chem.* **187**, 112004 (2020).
15. in, D. M.-C. S. H. perspectives & 2012, undefined. MAP kinase pathways. *cshperspectives.cshlp.org*.
16. M H Cobb *et al.* Regulation of the MAP kinase cascade - PubMed. *Cell Mol Biol Res.* **3**, 253–256 (1994).
17. Owens, D. M. & Keyse, S. M. Differential regulation of MAP kinase signalling by dual-specificity protein phosphatases. *Oncogene* vol. 26 3203–3213 (2007).
18. Cuadrado, A. & Nebreda, A. R. Mechanisms and functions of p38 MAPK signalling. *Biochemical Journal* vol. 429 403–417 (2010).

19. Wang, Z. *et al.* The structure of mitogen-activated protein kinase p38 at 2.1-Å resolution. *Proc. Natl. Acad. Sci. U. S. A.* **94**, 2327–2332 (1997).
20. Zhang, F., Strand, A., Robbins, D., Cobb, M. H. & Goldsmith, E. J. Atomic structure of the MAP kinase ERK2 at 2.3 Å resolution. *Nature* **367**, 704–711 (1994).
21. Bardwell, A. J., Frankson, E. & Bardwell, L. Selectivity of docking sites in MAPK kinases. *J. Biol. Chem.* **284**, 13165–13173 (2009).
22. Saxena, M., Williams, S., Brockdorff, J., Gilman, J. & Mustelin, T. Inhibition of T cell signaling by mitogen-activated protein kinase- targeted hematopoietic tyrosine phosphatase (HePTP). *J. Biol. Chem.* **274**, 11693–11700 (1999).
23. Roulston, A., Reinhard, C., Amiri, P. & Williams, L. T. *Early Activation of c-Jun N-terminal Kinase and p38 Kinase Regulate Cell Survival in Response to Tumor Necrosis Factor* \*. <http://www.jbc.org/> (1998).
24. Bradham, C. & McClay, D. R. p38 MAPK in development and cancer. *Cell Cycle* vol. 5 824–828 (2006).
25. K, T. *et al.* ASK1 is required for sustained activations of JNK/p38 MAP kinases and apoptosis. *EMBO Rep.* **2**, (2001).
26. Rheumatoid Arthritis (RA) | Arthritis | CDC. *National Center for Chronic Disease Prevention and Health* <https://www.cdc.gov/arthritis/basics/rheumatoid-arthritis.html> (2020).
27. Korb, A. *et al.* Differential tissue expression and activation of p38 MAPK  $\alpha$ ,  $\beta$ ,  $\gamma$ , and  $\delta$  isoforms in rheumatoid arthritis. *Arthritis Rheum.* **54**, 2745–2756 (2006).

28. Ho, F. & Khalil, H. Crohn's disease: A clinical update. *Therapeutic Advances in Gastroenterology* vol. 8 352–359 (2015).
29. Hanahan, D. & Weinberg, R. A. The Hallmarks of Cancer Review evolve progressively from normalcy via a series of pre. *Cell* **100**, 57–70 (2000).
30. Bulavin, D. V. & Fornace, A. J. p38 MAP kinase's emerging role as a tumor suppressor. *Adv. Cancer Res.* **92**, 95–118 (2004).
31. Wang, W. *et al.* Sequential Activation of the MEK-Extracellular Signal-Regulated Kinase and MKK3/6-p38 Mitogen-Activated Protein Kinase Pathways Mediates Oncogenic ras-Induced Premature Senescence. *Mol. Cell. Biol.* **22**, 3389–3403 (2002).
32. MAPK14 (mitogen-activated protein kinase 14).  
[http://atlasgeneticsoncology.org/Genes/GC\\_MAPK14.html](http://atlasgeneticsoncology.org/Genes/GC_MAPK14.html).
33. Kallunki, T. *et al.* *JNK2 contains a specificity-determining region responsible for efficient c-Jun binding and phosphorylation.* (1994).
34. Chang, C. I., Xu, B. E., Akella, R., Cobb, M. H. & Goldsmith, E. J. Crystal structures of MAP kinase p38 complexed to the docking sites on its nuclear substrate MEF2A and activator MKK3b. *Mol. Cell* **9**, 1241–1249 (2002).
35. Zhou, T., Sun, L., Humphreys, J. & Goldsmith, E. J. Docking Interactions Induce Exposure of Activation Loop in the MAP Kinase ERK2. *Structure* **14**, 1011–1019 (2006).

36. Muñoz, J. J., Muñoz, M., Arrega, C. T. ', Blanco-Aparicio, C. & Pulido, R. *Differential interaction of the tyrosine phosphatases PTP-SL, STEP and HePTP with the mitogen-activated protein kinases ERK1/2 and p38 $\alpha$  is determined by a kinase specificity sequence and influenced by reducing agents. Biochem. J* vol. 372 (2003).
37. Blanco-Aparicio, C., Muñoz, J. J. & Pulido, R. Two Clusters of Residues at the Docking Groove of Mitogen-activated Protein Kinases Differentially Mediate Their Functional Interaction with the Tyrosine Phosphatases PTP-SL and STEP\* Cé line Tá rrega. (2001) doi:10.1074/jbc.M108874200.
38. White, A., Pargellis, C. A., Studts, J. M., Werneburg, B. G. & Farmer, B. T. Molecular basis of MAPK-activated protein kinase 2:p38 assembly. *Proc. Natl. Acad. Sci. U. S. A.* **104**, 6353–6358 (2007).
39. Garai, Á. *et al.* Specificity of linear motifs that bind to a common mitogen-activated protein kinase docking groove. *Sci. Signal.* **5**, (2012).
40. Kokoette, B. & Sekelwa, C. Antiuropathogenic and antioxidant activities of Hypoxis hemerocallidea Lam. extracts, and compounds from its taxonomically related species. *Arch. Pharm. Pharm. Sci.* **4**, 001–009 (2020).
41. Mills, E., Cooper, C., Seely, D. & Kanfer, I. African herbal medicines in the treatment of HIV: Hypoxis and Sutherlandia. An overview of evidence and pharmacology. *Nutrition Journal* vol. 4 1–6 (2005).
42. Drewes, S. E., Hall, A. J., Learmonth, R. A. & Upfold, U. J. Isolation of hypoxoside from hypoxis rooperi and synthesis of (E)-1,5-bis(3',4'-dimethoxyphenyl)pent-4-en-1-yne. *Phytochemistry* **23**, 1313–1316 (1984).

43. Oguntibeju, O. O., Meyer, S., Aboua, Y. G. & Goboza, M. Hypoxis hemerocallidea Significantly Reduced Hyperglycaemia and Hyperglycaemic-Induced Oxidative Stress in the Liver and Kidney Tissues of Streptozotocin-Induced Diabetic Male Wistar Rats. *Evidence-based Complement. Altern. Med.* **2016**, (2016).
44. Ojewole, J. A. O. Antinociceptive, anti-inflammatory and antidiabetic properties of Hypoxis hemerocallidea Fisch. & C.A. Mey. (Hypoxidaceae) corm [‘African Potato’] aqueous extract in mice and rats. *J. Ethnopharmacol.* **103**, 126–134 (2006).
45. Bettolo, G. B. M., Patamia, M., Nicoletti, M., Galeffi, C. & Messana, I. Research on African medicinal plants-II. Hypoxoside, a new glycoside of uncommon structure from hypoxis obtusa busch. *Tetrahedron* **38**, 1683–1687 (1982).
46. Albrecht, C. F., Theron, E. J. & Kruger, P. Morphological characterisation of the cell-growth inhibitory activity of rooperol and pharmacokinetic aspects of hypoxoside as an oral prodrug for cancer therapy - PubMed. *S Afr Med J* **9**, 853–860 (1995).
47. Bohanon, A., Kerwin, S. M., David, W. & Du, L. STABILITY STUDIES OF ROOPEROL AND ANALOGUES BY IN VITRO METABOLISM WITH HPLC/MS DETECTION. (Texas State University, 2019).
48. Smit, B. j *et al.* A phase I trial of hypoxoside as an oral prodrug for cancer therapy -absence of toxicity - PubMed. *S Afr Med J* . 865–870 (1995).

49. Theron, E. J., Albrecht, C. F., Kruger, P. B., Jenkins, K. & Van der Merwe, M. J.  $\beta$ -Glucosidase activity in fetal bovine serum renders the plant glucoside, hypoxoside, cytotoxic toward B16-F10-BL-6 mouse melanoma cells. *Vitr. Cell. Dev. Biol. - Anim. J. Soc. Vitr. Biol.* **30**, 115–119 (1994).
50. Boukes, G. J., Daniels, B. B., Albrecht, C. F. & Van de Venter, M. Cell survival or apoptosis: Rooperol's role as anticancer agent. *Oncol. Res.* **18**, 365–376 (2010).
51. Li, J. *et al.* A Fluorescence-Based Assay for p38 $\alpha$  Recruitment Site Binders: Identification of Rooperol as a Novel p38 $\alpha$  Kinase Inhibitor. *ChemBioChem* **14**, 66–71 (2013).
52. Brown, N. *Bioisosteres in Medicinal Chemistry. Bioisosteres in Medicinal Chemistry* vol. 54 (Wiley Blackwell, 2012).
53. Cho, S. Y., Kim, M. K., Mok, H., Choo, H. & Chong, Y. Separation of quercetin's biological activity from its oxidative property through bioisosteric replacement of the catecholic hydroxyl groups with fluorine atoms. *J. Agric. Food Chem.* **60**, 6499–6506 (2012).
54. Kerwin, S. M. & Cha, J. A concise synthesis of rooperol and related 1,5-diarylpent-1-en-4-yne. *Tetrahedron Lett.* **55**, 137–141 (2014).
55. Kontoyianni, M. Docking and virtual screening in drug discovery. in *Methods in Molecular Biology* vol. 1647 255–266 (Humana Press Inc., 2017).
56. Alvarez, J. & Shoichet, B. *Virtual Screening in Drug Discovery*. (Taylor & Francis Group, 2005).
57. Patrick Walters, W., Stahl, M. T. & Murcko, M. A. Virtual screening - An overview. *Drug Discov. Today* **3**, 160–178 (1998).

58. Mason, J., Good, A. & Martin, E. 3-D Pharmacophores in Drug Discovery. *Curr. Pharm. Des.* **7**, 567–597 (2005).
59. Lyne, P. D. Structure-based virtual screening: An overview. *Drug Discovery Today* vol. 7 1047–1055 (2002).
60. Gagic, Z., Ruzic, D., Djokovic, N., Djikic, T. & Nikolic, K. In silico Methods for Design of Kinase Inhibitors as Anticancer Drugs. *Frontiers in Chemistry* vol. 7 (2020).
61. Muegge, I. & Rarey, M. Small molecule docking and scoring. *Rev. Comput. Chem.* **17**, 1–60 (2001).
62. Pagadala, N. S., Syed, K. & Tuszynski, J. Software for molecular docking: a review. *Biophysical Reviews* vol. 9 91–102 (2017).
63. Kinase.com. <http://kinase.com/web/current/>.
64. Kanev, G. K., de Graaf, C., Westerman, B. A., de Esch, I. J. P. & Kooistra, A. J. KLIFS: An overhaul after the first 5 years of supporting kinase research. *Nucleic Acids Res.* **49**, D562–D569 (2021).
65. Bajusz, D., Ferenczy, G. G. & Keseru, G. M. Discovery of Subtype Selective Janus Kinase (JAK) Inhibitors by Structure-Based Virtual Screening. *J. Chem. Inf. Model.* **56**, 234–247 (2016).
66. Lang, C. A., Ray, S. S., Liu, M., Singh, A. K. & Cuny, G. D. Discovery of LRRK2 inhibitors using sequential in silico joint pharmacophore space (JPS) and ensemble docking. *Bioorganic Med. Chem. Lett.* **25**, 2713–2719 (2015).
67. Muegge, I. & Enyedy, I. J. Virtual Screening for Kinase Targets. *Curr. Med. Chem.* **11**, 693–707 (2005).

68. Ma, H., Deacon, S. & Horiuchi, K. The challenge of selecting protein kinase assays for lead discovery optimization. *Expert Opinion on Drug Discovery* vol. 3 607–621 (2008).
69. Hastie, C. J., McLauchlan, H. J. & Cohen, P. Assay of protein kinases using radiolabeled ATP: A protocol. *Nat. Protoc.* **1**, 968–971 (2006).
70. Smyth, L. A. & Collins, I. Measuring and interpreting the selectivity of protein kinase inhibitors. *Journal of Chemical Biology* vol. 2 131–151 (2009).
71. Olive, M. & Biosciences, L. Quantitative methods for analysis of protein phosphorylation in drug development. *Expert Rev. Proteomics* **3**, (2004).
72. Ter Haar, E., Prabakhar, P., Liu, X. & Lepre, C. Crystal structure of the P38 $\alpha$ -MAPKAP kinase 2 heterodimer. *J. Biol. Chem.* **282**, 9733–9739 (2007).
73. Honndorf, V. S. *et al.* Inferential NMR/X-ray-based structure determination of a dibenzo[a,d]cycloheptenone inhibitor-p38 $\alpha$  MAP kinase complex in solution. *Angew. Chemie - Int. Ed.* **51**, 2359–2362 (2012).
74. Wang, Z. *et al.* Structural basis of inhibitor selectivity in MAP kinases. *Structure* **6**, 1117–1128 (1998).
75. Zhang, Y. Y., Wu, J. W. & Wang, Z. X. A distinct interaction mode revealed by the crystal structure of the kinase p38 $\alpha$  with the MAPK binding domain of the phosphatase MKP5. *Sci. Signal.* **4**, (2011).
76. Haan, C. & Behrmann, I. A cost effective non-commercial ECL-solution for Western blot detections yielding strong signals and low background. *J. Immunol. Methods* **318**, 11–19 (2007).

77. Opentrons | Open-source Lab Automation, starting at \$5,000 | Opentrons.  
[https://opentrons.com/?utm\\_source=adwords&utm\\_campaign=Branded&utm\\_term=open trons&utm\\_medium=ppc&hsa\\_tgt=kwd-435242170207&hsa\\_cam=881433800&hsa\\_acc=2303351826&hsa\\_kw=open trons&hsa\\_mt=e&hsa\\_src=g&hsa\\_grp=58894000297&hsa\\_ad=328563245402&hsa\\_ver=3&hsa\\_net=adwords&gclid=CjwKCAjw\\_JuGBhBkEiwA1xmbRcPuE9JiilpHRidcjhQ5X0XSHcFaNoR6BcOSuZ905IMVn6d2RH5BdRoC5GYQAvD\\_BwE](https://opentrons.com/?utm_source=adwords&utm_campaign=Branded&utm_term=open+trons&utm_medium=ppc&hsa_tgt=kwd-435242170207&hsa_cam=881433800&hsa_acc=2303351826&hsa_kw=open+trons&hsa_mt=e&hsa_src=g&hsa_grp=58894000297&hsa_ad=328563245402&hsa_ver=3&hsa_net=adwords&gclid=CjwKCAjw_JuGBhBkEiwA1xmbRcPuE9JiilpHRidcjhQ5X0XSHcFaNoR6BcOSuZ905IMVn6d2RH5BdRoC5GYQAvD_BwE).
78. Zegzouti, H., Zdanovskaia, M., Hsiao, K. & Goueli, S. A. ADP-Glo: A bioluminescent and homogeneous adp monitoring assay for Kinases. *Assay Drug Dev. Technol.* **7**, 560–572 (2009).
79. JH, Z., TD, C. & KR, O. A Simple Statistical Parameter for Use in Evaluation and Validation of High Throughput Screening Assays. *J. Biomol. Screen.* **4**, 67–73 (1999).
80. Corporation, P. *Using the Kinase Enzyme Systems with the ADP-Glo<sup>TM</sup> Assay Technical Manual, TM553*. www.promega.com (2019).
81. Laboratories, B.-R. Image Lab Software User Guide. (2020).